Dynamic localization of a yeast development specific PP1 complex during prospore membrane formation is dependent on multiple localization signals and complex formation

doi: 10.1091/mbc.E17-08-0521

Dynamic localization of a yeast development–specific PP1 complex during prospore membrane formation is dependent on multiple localization signals and complex formation

Tsuyoshi S. Nakamura[a], Yumi Numajiri[a], Yuuya Okumura[a], Junji Hidaka[a], Takayuki Tanaka[a], Ichiro Inoue[a], Yasuyuki Suda[b], Tetsuo Takahashi[c], Hideki Nakanishi[d], Xiao-Dong Gao[d], Aaron M. Neiman[e], and Hiroyuki Tachikawa[a,*]

[a]Department of Applied Biological Chemistry, Graduate School of Agricultural and Life Sciences, The University of Tokyo, Tokyo 113-8657, Japan; [b]Department of Molecular Cell Biology, Graduate School of Comprehensive Human Sciences and Institute of Basic Medical Sciences, University of Tsukuba, Ibaraki 305-8575, Japan; [c]Laboratory of Glycobiology and Glycotechnology, Department of Applied Biochemistry, School of Engineering, Tokai University, Kanagawa 259-1292, Japan; [d]Key Laboratory of Carbohydrate Chemistry and Biotechnology, Ministry of Education, School of Biotechnology, Jiangnan University, Wuxi 214122, China; [e]Department of Biochemistry and Cell Biology, Stony Brook University, Stony Brook, NY 11794-5215

ABSTRACT **During the developmental process of sporulation in *Saccharomyces cerevisiae*, membrane structures called prospore membranes are formed de novo, expand, extend, acquire a round shape, and finally become plasma membranes of the spores. *GIP1* encodes a regulatory/targeting subunit of protein phosphatase type 1 that is required for sporulation. Gip1 recruits the catalytic subunit Glc7 to septin structures that form along the prospore membrane; however, the molecular basis of its localization and function is not fully understood. Here we show that Gip1 changes its localization dynamically and is required for prospore membrane extension. Gip1 first associates with the spindle pole body as the prospore membrane forms, moves onto the prospore membrane and then to the septins as the membrane extends, distributes around the prospore membrane after closure, and finally translocates into the nucleus in the maturing spore. Deletion and mutation analyses reveal distinct sequences in Gip1 that are required for different localizations and for association with Glc7. Binding to Glc7 is also required for proper localization. Strikingly, localization to the prospore membrane, but not association with septins, is important for Gip1 function. Further, our genetic analysis suggests that a Gip1–Glc7 phosphatase complex regulates prospore membrane extension in parallel to the previously reported Vps13, Spo71, Spo73 pathway.**

Monitoring Editor
Patrick J. Brennwald
University of North Carolina

Received: Aug 21, 2017
Revised: Oct 6, 2017
Accepted: Oct 10, 2017

INTRODUCTION

Sporulation of *Saccharomyces cerevisiae* is a developmental process in which dynamic cellular reorganization occurs. In response to nutrient limitation, spores are formed in the cytoplasm of the original diploid cell, which is then termed an ascus. Spores allow survival in severe environmental situations. Spore formation is coordinated with the meiotic divisions (Moens, 1971; Kupiec *et al.*, 1997;

This article was published online ahead of print in MBoC in Press (http://www.molbiolcell.org/cgi/doi/10.1091/mbc.E17-08-0521) on October 18, 2017.

Author contributions: H.T. and A.M.N. conceived and designed experiments; T.S.N., Y.N., Y.O., J.H., T.T., I.I., Y.S., T.T., H.N., and H.T. performed the experiments and analyzed the data; T.S.N., X.G., A.M.N., and H.T. interpreted the data and drafted the article; T.S.N. prepared digital images.

*Address correspondence to: Hiroyuki Tachikawa (atachi@mail.ecc.u-tokyo.ac.jp).

Abbreviations used: CIAP, calf intestine alkaline phosphatase; DIC, differential interference contrast; GFP, green fluorescent protein; LEC, leading edge complex; PMSF, phenylmethylsulfonyl fluoride; PP1, protein phosphatase type 1; PSM, prospore membrane; SD, synthetic dextrose; SNARE, soluble NSF attachment protein receptor; SPB, spindle pole body; TCA, trichloroacetic acid; YPD, yeast extract–peptone–dextrose.

Supplemental Material can be found at:
http://www.molbiolcell.org/content/suppl/2017/10/16/mbc.E17-08-0521v1.DC1

Neiman, 1998, 2005, 2011). During meiosis II, double membrane structures called prospore membranes appear at the cytoplasmic surface of each spindle pole body (SPB) and expand to form small round membranes, enveloping the daughter nuclei that are produced through meiosis. Prospore membranes then extend into a tube-like elongated shape to encapsulate organelles and cytosol. We call this stage "prospore membrane extension." At the end of meiosis II, prospore membranes close and form spheres, and then spore walls are deposited between the double membranes. Because the prospore membrane is formed de novo, it is a good model for membrane formation in the cell.

Molecular mechanisms of each stage of prospore membrane formation and growth have been described (Neiman, 2011). Early in meiosis II, SPB modification occurs prior to membrane formation; components of the outer plaque of each SPB are replaced with sporulation-specific components, and the meiosis II outer plaque is formed (Knop and Strasser, 2000; Bajgier *et al.*, 2001; Nickas *et al.*, 2003). There, secretory vesicles are tethered and fused to form prospore membranes, a process that is dependent on sporulation-specific SNARE complex and phospholipase D, Spo14 (Nakanishi *et al.*, 2004, 2006; Mathieson *et al.*, 2010). Prospore membranes expand to form small, round caps over the SPBs by further fusion of secretory vesicles and then extend into a tube-like shape. Two membrane-associated protein structures are formed at this stage: the leading edge complex (LEC) and the septin structure. The LEC consists of at least four proteins, localizes to the lip of the prospore membrane, and is required for proper prospore membrane extension (Moreno-Borchart *et al.*, 2002; Nickas and Neiman, 2002; Lam *et al.*, 2014). Septins are a conserved family of proteins that form filaments. In vegetative cells, Cdc10, Cdc3, Cdc12, and Cdc11 or Shs1 form hetero-octamers that assemble into a ring at the bud neck (Bertin *et al.*, 2008, 2012). During sporulation, Spr3 and Spr28 are induced and substitute for Cdc12 and Shs1/Cdc11, and the resulting sporulation-specific septin complex forms parallel bars along the prospore membrane (De Virgilio *et al.*, 1996; Fares *et al.*, 1996; Garcia *et al.*, 2016). These sporulation-specific septin structures are required for prospore membrane extension, at least in some strains (Heasley and McMurray, 2016). Extension of the prospore membrane requires *VPS13*, *SPO71*, and *SPO73* (Park and Neiman, 2012; Parodi *et al.*, 2012, 2015; Okumura *et al.*, 2016). Loss of any of these genes causes prospore membrane growth to stop at the small round stage. Spo71 recruits Vps13 to the prospore membrane and also interacts with Spo73 (Park *et al.*, 2013; Okumura *et al.*, 2016). Although the precise mechanisms by which these proteins work are still unknown, the proteins are thought to form a complex on the prospore membrane and to facilitate membrane extension.

Glc7 is the only catalytic subunit of protein phosphatase type 1 (PP1) in *S. cerevisiae*. PP1 is a conserved protein and is involved in a variety of cellular processes, for which it is recruited by different regulatory/targeting subunits (Bollen *et al.*, 2010). In yeast, Glc7 functions in multiple processes, including glucose repression with Reg1, glycogen synthesis with Gac1, endocytosis with Scd5, and cell wall synthesis during cytokinesis with Bni4 (Stuart *et al.*, 1994; Tu and Carlson, 1995; Kozubowski *et al.*, 2003; Cannon, 2010; Chi *et al.*, 2012). Glc7 functions in sporulation with Gip1.

Gip1 was originally isolated in a screen to identify interacting proteins of Glc7 and is a sporulation-specific protein required for sporulation (Tu *et al.*, 1996). During prospore membrane formation, Gip1–Glc7 localizes to the septin bars along the prospore membrane, and after closure of the prospore membrane, Gip1 localizes uniformly around the membrane (Tachikawa *et al.*, 2001). Analysis of *gip1*Δ cells revealed that Gip1 is required for proper localization of Glc7, septin organization, and spore wall formation (Tachikawa *et al.*, 2001). Expression of a Glc7 mutant defective in binding to Gip1 as the sole Glc7 protein causes a phenotype similar to *gip1*Δ (Tachikawa *et al.*, 2001). Thus, Gip1 is considered to be a sporulation-specific targeting subunit of Glc7; however, the molecular basis of its function and localization is not fully understood. *YSW1* gene was identified as a multicopy suppressor of *gip1* temperature-sensitive allele, and Ysw1 protein was shown to interact with Gip1 (Ishihara *et al.*, 2009). Ysw1 localizes to the septin bars in a *GIP1*-dependent manner, and deletion of the *YSW1* gene causes a defect in prospore membrane formation, but the sporulation defect is much weaker than that of the *gip1*Δ mutant (Ishihara *et al.*, 2009).

In this study, we carefully revisit the *gip1*Δ phenotype and Gip1 localization and show that *GIP1* is required for prospore membrane extension and that Gip1 localization is dynamic during sporulation. Deletion and mutation analyses reveal different domains of Gip1 to be required for its function and recruitment to various cellular locations. Further, our data suggest that Gip1 functions in prospore membrane extension in parallel to the previously reported Vps13, Spo71, Spo73 pathway. Our data support the existence of a novel regulation of prospore membrane extension by the Gip1–Glc7 phosphatase complex.

RESULTS

Gip1 is required for prospore membrane extension

The localization of Gip1 to septin structures along the extending prospore membrane (Tachikawa *et al.*, 2001), together with the evidence that a deletion of *YSW1*, encoding a Gip1 interacting protein, causes a partial defect in prospore membrane formation (Ishihara *et al.*, 2009), led us to examine whether prospore membranes are properly formed in the *gip1*Δ mutant. A fusion of residues 51–91 of Spo20 with green fluorescent protein (GFP) was used as a prospore membrane marker (Nakanishi *et al.*, 2004) and was expressed in *gip1*Δ cells during sporulation. Prospore membranes in *gip1*Δ mutants appeared smaller than those in wild-type cells (Figure 1A). To quantify the difference in prospore membrane size, Htb2 tagged with mCherry was used as a nuclear marker (Okumura *et al.*, 2016) to identify post-meiotic cells and the perimeter lengths of prospore membranes were measured (Figure 1B). The results indicate that prospore membranes in *gip1*Δ mutant cells are smaller than those in wild-type cells (Figure 1C), with most of the prospore membranes successfully capturing nuclei (>90%). As prospore membranes grow, they move through a series of discrete morphologies (Diamond *et al.*, 2009). Initially, they appear as small caps on the spindle pole bodies; these expand into round structures and then extend into elongated shapes before becoming round again at prospore membrane closure. Time-lapse analysis of prospore membrane growth in the *gip1*Δ mutant revealed that prospore membrane formation initiates properly, but extension of prospore membranes into elongated shapes is rarely seen (Figure 1D and Supplemental Movies S1 and S2). These observations indicate that Gip1 is required for prospore membrane extension.

Gip1 dynamically changes its localization during prospore membrane formation

Gip1 localization during sporulation was previously analyzed using an N-terminally hemagglutinin-tagged version of Gip1 (HA-Gip1) in fixed cells (Tachikawa *et al.*, 2001). To analyze the localization in live cells, we constructed *GIP1-GFP* based on the DNA sequence of the *GIP1* gene at the *Saccharomyces* Genome Database (SGD), which was revised in a resequencing project (Engel *et al.*, 2014). Although *GIP1-GFP* expressed using a CEN-based low-copy-number vector rescued the sporulation defect of the *gip1*Δ mutant, no

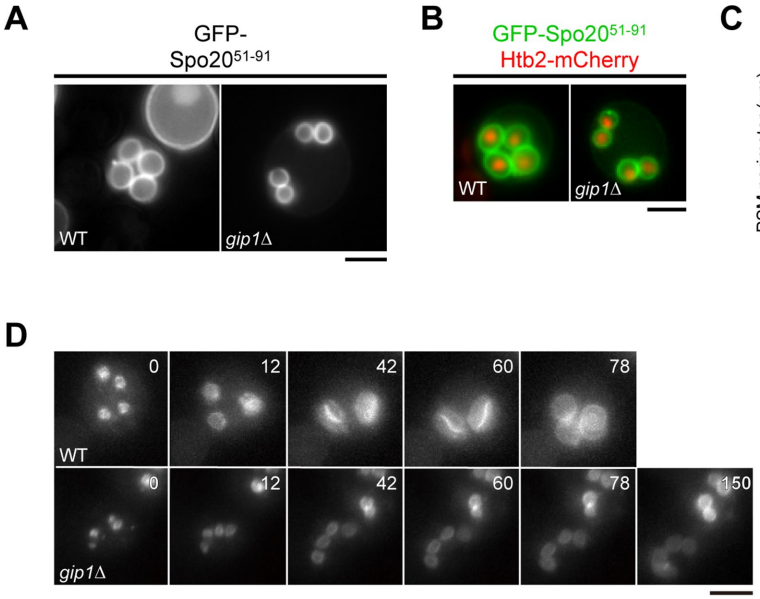

FIGURE 1: Observation of prospore membranes in wild-type and *gip1*Δ cells. (A) AN120 (wild-type) and TC544 (*gip1*Δ) cells were transformed with pRS424-P_{TEF1}-GFP-SPO20$^{51–91}$, sporulated for 7 h, and subjected to fluorescence microscopy. (B, C) Representative images (B) and prospore membrane perimeters (C) of postmeiotic cells of strains AN120 (wild type) and TC544 (*gip1*Δ) carrying pRS424-P_{TEF1}-GFP-SPO20$^{51–91}$, and pRS316-HTB2-mCherry are shown as the mean ± the SD. More than 50 PSMs were examined in three independent colonies of each strain (for a total of >150 PSMs). ***$P < 0.001$ (Student's *t* test). (D) AN120 (wild-type) and TC544 (*gip1*Δ) cells were transformed with pRS424-P_{TEF1}-GFP-SPO20$^{51–91}$, sporulated for 7 h, and subjected to time-lapse microscopic analysis. The time after the start of observation is shown in minutes. In all images, scale bars indicate 5 μm.

GFP fluorescence was observed (unpublished data). Thus, we overexpressed *GIP1-GFP* using a multicopy vector. In addition to the septin localization seen in the earlier immunofluorescence study (Tachikawa *et al.*, 2001), Gip1-GFP showed localization to small prospore membranes, large round prospore membranes, and nuclei (Figure 2A), which was confirmed by colocalization with respective markers (Figure 2B). We also observed some dot patterns early in meiosis II; however, they did not colocalize with SPB or nucleolar markers (Schimmang *et al.*, 1989; Mathieson *et al.*, 2010) in most cells (Supplemental Figure S1, A and B). When Gip1-GFP was observed in an *sso1*Δ mutant, in which prospore membrane development arrests with precursor vesicles accumulated at the SPB, SPB localization of Gip1-GFP was observed (Supplemental Figure S1C), suggesting transient SPB localization in the wild type. It should be noted that we observed aberrantly narrow overextended prospore membranes in ~7.5% of the *gip1*Δ cells overexpressing Gip1-GFP, consistent with the model of Gip1 as involved in prospore membrane extension (Supplemental Figure S1D). Time-lapse analysis of Gip1-GFP revealed the order of change in localization (Figure 2, C and D, and Supplemental Movies S3–S5). Gip1 localizes first to small prospore membranes. As prospore membranes extend and septin bars are formed, Gip1 localizes to these septin structures. As prospore membranes become round at the time of closure, Gip1-GFP is seen transiently along the entire membrane, but then it is released from the membrane, moves into the nucleus, and finally disappears. These observations indicate that Gip1 localization is dynamic through spore formation.

Overexpression of the C-terminal region of Gip1 can partially rescue *gip1*Δ

Our data show that Gip1 localizes to various cellular locations and also functions in prospore membrane extension. To identify regions of Gip1 important for function and for targeting to different cellular locations, a deletion series of *GIP1* was constructed as a fusion to the GFP coding sequence (Figure 3A).

First, these deletions were overexpressed in *gip1*Δ cells to assess their functionality. In the C-terminal deletion series of Gip1, only Gip1-N8(1–589) was mostly functional. The *gip1*Δ mutant expressing Gip1-N1(1–67) to Gip1-N6(1–476) did not sporulate, and no prospore membrane extension was observed in those cells. Slight sporulation was observed in cells expressing Gip1-N7(1–518) (0.2%). As for the N-terminal deletions, all three are partially functional. The *gip1*Δ mutant expressing Gip1-C1(477–639), Gip1-C2(358–639), and Gip1-C3(133–639) showed 1.7%, 6.3%, and 10.3% sporulation, respectively. These results suggest that the region between residues 477 and 589 has an essential function for sporulation.

Distinct regions of Gip1 are required for targeting to different cellular locations

Next, the different deletions were overexpressed in wild-type and *gip1*Δ cells, and localization of each of the expressed proteins was observed (Figure 3B) with respect to a prospore membrane marker (Supplemental Figure S2) and other markers (Figure 3C) during meiosis II. In the C-terminal deletion series, Gip1-N1(1–67) showed a prospore membrane pattern with diffuse cytosolic localization, while Gip1-N2(1–132) localized clearly to prospore membrane in both wild-type and *gip1*Δ cells, suggesting the existence of a weak membrane localization signal between residues 1 and 67 of Gip1 and a strong membrane localization signal between residues 68 and 132. Gip1-N3(1–222) to N7(1–518) showed the septin pattern in wild-type cells indicating that residues 133–222 of Gip1 are required for septin association. In *gip1*Δ cells, in which no septin bars are observed (Tachikawa *et al.*, 2001), the fusions showed a small prospore membrane pattern. Gip1-N8(1–589), which is functional, showed the wild-type Gip1 localization pattern.

In the N-terminal deletion series, Gip1-C1(477–639) displayed a diffuse cytosolic pattern with dots in both meiosis II wild-type cells and *gip1*Δ cells (Figure 3B). More than 70% of these dots showed an SPB-like pattern and these dots colocalized with the meiotic SPB marker Mpc54-RFP (Figure 3C), indicating that the region between residues 477 and 639 of Gip1 confers the localization on the SPB. A similar pattern was observed with Gip1-C2(358–639) and Gip1-C3(133–639), although Gip1-C2 and -C3 are partially concentrated in the nucleus and Gip1-C3 also showed a filament-like pattern of variable direction and length (30% of cells).

In postmeiotic wild-type cells, while Gip1-N8 localized to the nucleus as well as full-length Gip1, Gip1-N6(1–476) localized to the prospore membrane (Supplemental Figure S2). Gip1-N7 showed localization to both the nucleus and the prospore membrane. These observations suggest that the region between residues 476 and 589 contains a sequence needed for release from the prospore membrane. Gip1-C2 and -C3 localized to the nucleus, as was the case with full-length Gip1 (Supplemental Figure S2); in contrast, Gip1-C1

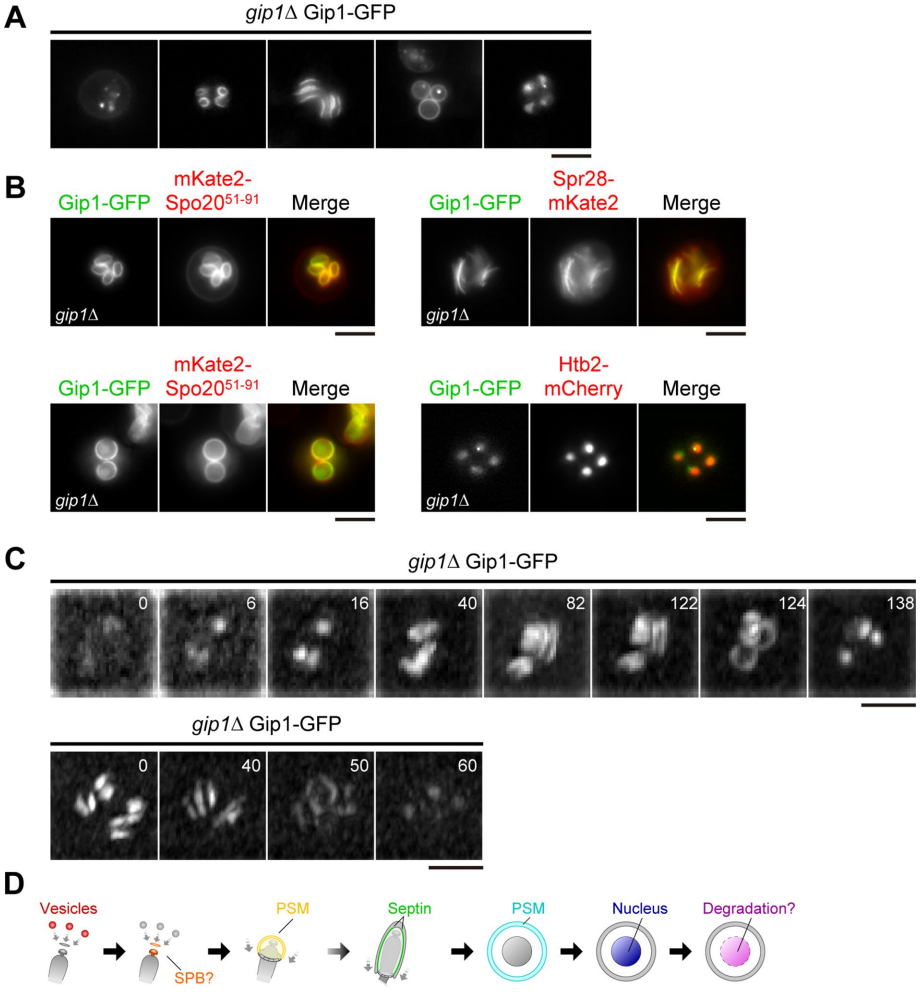

FIGURE 2: Localization of Gip1 during sporulation. (A) TC544 (*gip1*Δ) cells were transformed with pRS424-GIP1-GFP, sporulated, and observed at 7–9 h. (B) TC544 (*gip1*Δ) cells were transformed with pRS424-GIP1-GFP and pRS316-P_{TEF1}-mKate2-SPO20$^{51–91}$ (top left and bottom left), pRS316-SPR28-mKate2 (top right), or pRS316-HTB2-mCherry (bottom right), respectively, sporulated, and observed at 7–9 h. (C) TC544 (*gip1*Δ) cells were transformed with pRS424-GIP1-GFP, sporulated for 7 h, and subjected to time-lapse microscopic analysis. Top and bottom images indicate early to late and middle to late stages of prospore membrane formation, respectively. The time after the start of observation is shown in minutes. (D) Schematic diagram of the changes of Gip1 localization are shown. SPB: spindle pole body; PSM: prospore membrane. In all images, scale bars indicate 5 μm.

localized to the spore cytosol, suggesting that the region between residues 358 and 476 may contain a nuclear localization signal.

These results indicate that Gip1 contain multiple different targeting sequences throughout the protein that contribute to its dynamic localization; residues 1–132 to the prospore membrane, residues 133–222 to the septin bars, residues 358–476 to the nucleus, and residues 477–589 to the SPB. Residues 477–589 also contain a sequence required for postmeiotic release from the prospore membrane.

Two helices in the N-terminal region are necessary for efficient prospore membrane localization and are important for function of Gip1

Our deletion analysis revealed that both residues 1–67 and residues 68–132 contain sequences that can mediate prospore membrane localization. Amphipathic α-helices are a common membrane-binding motif (Segrest *et al.*, 1990), and each of these regions of Gip1 contains a predicted α-helix: helix1 (residues 8–25) has a basic surface and helix2 (residues 94–111) is amphipathic, having hydrophilic and hydrophobic surfaces (Figure 4A). To examine whether these helices contribute to membrane localization of Gip1, a mutational analysis was performed. Gip1-N1-BM (R17A, K18A; basic-to-alanine mutations) and Gip1-N1-HeM1 (K18P; a helix-breaking mutation) expressed in wild-type and *gip1*Δ cells localized to the cytosol, still showing a faint prospore membrane pattern during sporulation (Figure 4B and Supplemental Figure S3A). This indicates that helix1 is important, but there may be some additional affinity to prospore membranes in residues 1–67. Next, helix1 and helix2 were mutated in the context of Gip1-N2. The mutations HyM (F98E, L102E; hydrophobic-to-hydrophilic mutations) and HeM2 (L102P; a helix-breaking mutation) were introduced into helix2. While mutations in helix1 did not show any effect, mutations in helix2 modestly affected the localization of proteins, resulting in a cytosolic pattern with prospore membrane localization (Figure 4C and Supplemental Figure S3B). When Gip1-N2 was mutated in both helix1 and helix2, however, cytosolic localization dominated and only a faint prospore membrane pattern was observed in less than 30% of the cells, suggesting that these helices are important for membrane localization of Gip1 (Figure 4C). In postmeiotic wild-type cells, while Gip1-N2 localized to the prospore membrane, Gip1-N2 mutated in helix2 localized to the nucleus (Supplemental Figure S3B), indicating that Gip1-N2 can translocate into the nucleus when its interaction with the prospore membrane is disrupted by mutation of helix2. In the context of full-length Gip1, a mutation in helix2 was sufficient to disrupt Gip1 protein localization and to decrease sporulation efficiency (Figure 4, D and E, and Supplemental Figure S3C). These results suggest that of the two helices in the N-terminal region of Gip1, the amphipathic helix2 is especially required for efficient localization to the prospore membrane and thus for Gip1 function.

A region adjacent to the C-terminus of the amphipathic helix is required for septin localization of Gip1, but dispensable for Gip1 function

To refine the region required for septin localization, an additional deletion series of *GIP1* was constructed as a fusion to the GFP coding sequence and expressed in wild-type cells (Figure 5, A and B). While Gip1-N2d(1–209) showed a septin pattern, Gip1-N2a(1–150), Gip1-N2b(1–177), and Gip1-N2c(1–187) showed prospore membrane patterns. This indicates that the region between residues 188 and 209 or the sequence around residue 188 is required for Gip1 to colocalize with septins. An internal deletion removing this region (residues 178–222) from full-length *GIP1-GFP*, *GIP1-Δsep* mutant,

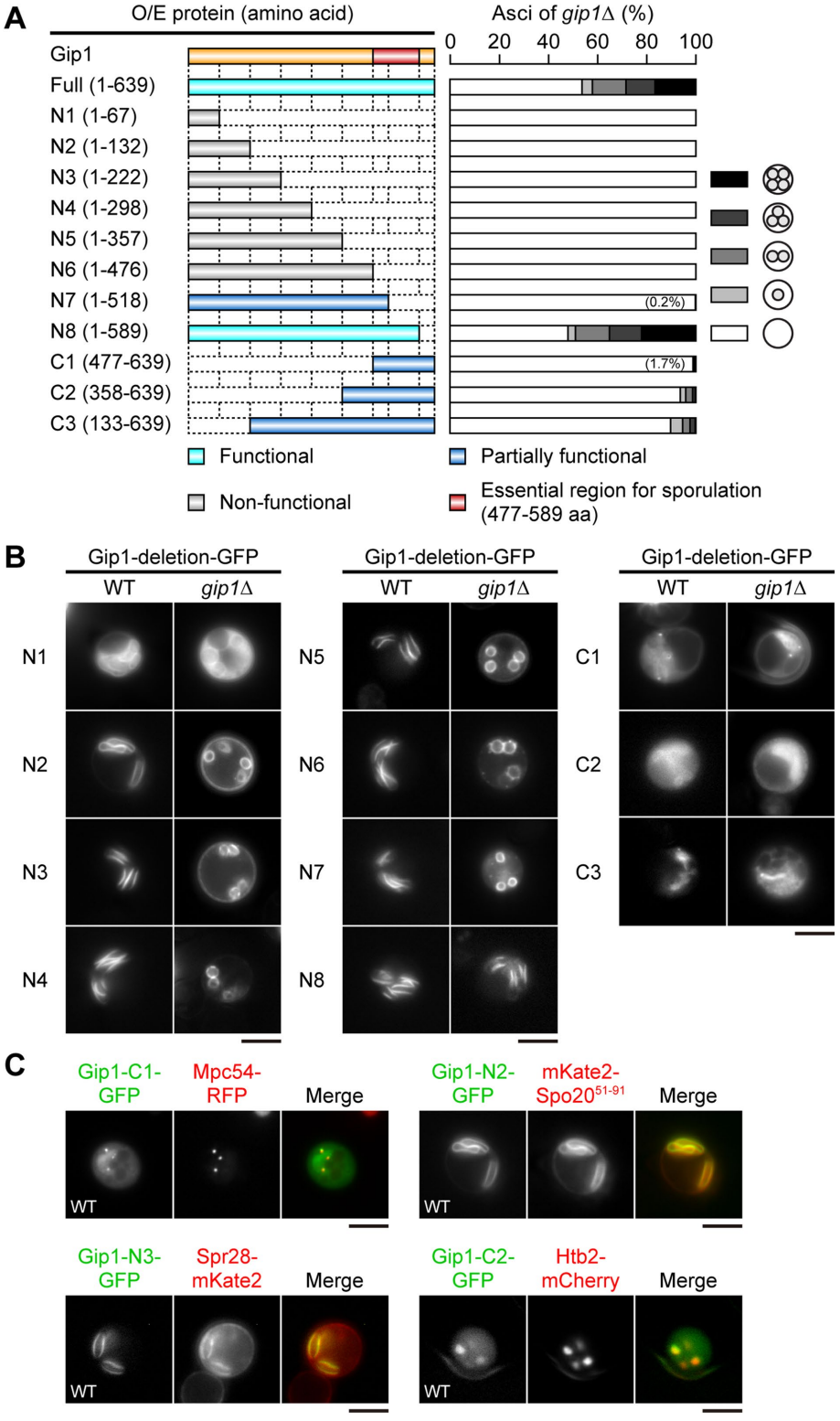

FIGURE 3: Analysis of Gip1-deletion mutants. (A) Left: Schematic diagram of Gip1-deletion mutants is shown. Light blue: functional, blue: partially functional, gray: nonfunctional, red: essential region for sporulation (residues 477–589). Right: TC544 (*gip1*Δ) cells were transformed with pRS424-GIP-deletion-mutant-GFP coding for indicated mutants, sporulated for 24 h, and observed with DIC microscopy. Percentages of asci are shown in the diagram. More than 200 cells were observed in three independent colonies of each strain harboring indicated deletion mutants (for a total of >600 cells). (B) AN120 (wild type) and TC544 (*gip1*Δ) were transformed with pRS424-GIP deletion mutant-GFP coding for indicated mutants and pRS316-P_{TEF1}-mKate2-SPO20$^{51–91}$, sporulated, and observed at 7–9 h. Only green fluorescent images of representative cells are shown. Red fluorescent and merged images are shown in Supplemental Figure S2. (C) AN120 (wild-type) cells were transformed with pRS424-GIP1-C1-GFP and pRS316-MPC54-RFP (top left), pRS424-GIP1-N2-GFP and pRS316-P_{TEF1}-mKate2-SPO20$^{51–91}$ (top right), pRS424-GIP1-N3-GFP and pRS316-SPR28-mKate2 (bottom left), or pRS424-GIP1-C2-GFP and pRS316-HTB2-mCherry (bottom right), respectively, sporulated, and observed at 7–9 h. Representative cells are shown. In all images, scale bars indicate 5 μm.

was constructed and expressed in the *gip1*Δ cells (Figure 5C). Gip1-Δsep did not localize to septin bars during membrane extension; instead it localized to the prospore membrane (Figure 5D). Importantly, septin organization appeared normal in these *GIP1-Δsep* cells (Figure 5E). In fact, Gip1-Δsep appeared fully functional. Cells expressing this protein sporulated as well as cells expressing full-length Gip1, even when expressed from a low copy vector (Figure 5F). These results indicate that septin localization of Gip1 is necessary neither for its function during prospore membrane extension nor for its role in organizing the septins. This is consistent with the observation that Gip1-GFP localizes uniformly on the prospore membrane in both the *spr3*Δ and *spr28*Δ mutant cells (Figure 5G), which show only modest sporulation defects in the SK1 strain background. We note that *gip1*Δ cells expressing Gip1-Δsep-GFP display disorganized prospore membranes in ~30% of the cells (Supplemental Figure S4), although the percentage of sporulation is similar to that in those expressing wild-type Gip1, reminiscent of a prospore membrane formation defect reported in septin mutants in the SK-BY background (Heasley and McMurray, 2016).

The region for septin localization was further examined using short fragments of Gip1 fused to GFP (Figure 5H). Although Gip1-SEP1 (residues 178–222) could not localize to septins (Figure 5I), a larger fragment, Gip1-SEP2 (residues 133–222), localized to the septin bars (Figure 5J), indicating that this domain contains a septin localization signal. Moreover, Gip1-SEP2 did not localize to the septin structure at the bud neck in vegetative cells (Figure 5K), suggesting that this localization signal is specific to the septin structure formed during sporulation.

Multiple nuclear localization signals (NLSs) contribute to postmeiotic nuclear localization of Gip1

Analysis of the localization of Gip1 deletion series revealed that the region

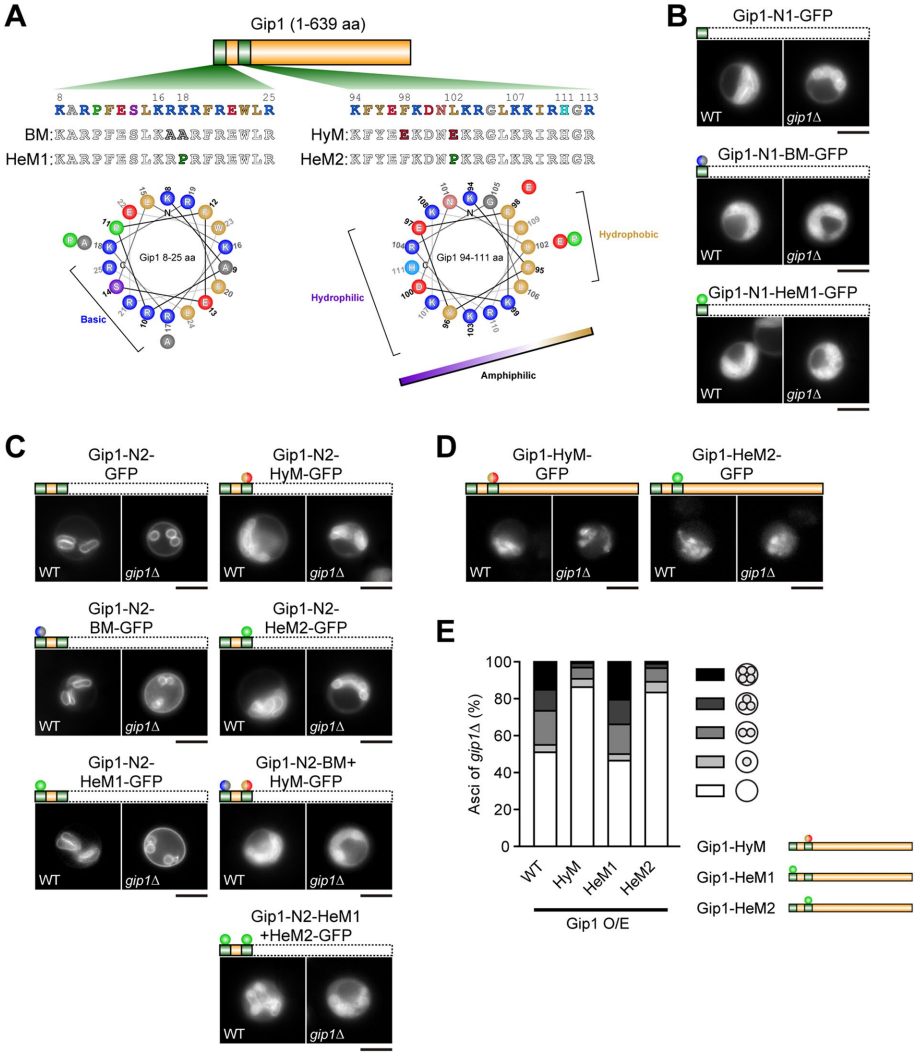

FIGURE 4: Analysis of two α-helices in the Gip1 N-terminal region. (A) Schematic diagram of two α-helices in the Gip1 N-terminal region is shown. Dark green: α-helix, BM: basic residue mutation, HyM: hydrophobic surface mutation, HeM: α-helix mutation. (B–D) AN120 (wild-type) and TC544 (*gip1*Δ) cells were transformed with pRS424-GIP1-N1-mutant-GFP (B), pRS424-GIP1-N2-mutant-GFP (C), and pRS424-GIP1-mutant-GFP (D), coding for indicated mutants, and pRS316-P_{TEF1}-mKate2-SPO20$^{51–91}$, sporulated, and observed at 7–9 h. Only green fluorescent images of representative cells are shown. Red fluorescent and merged images are shown in Supplemental Figure S3. Blue and gray: basic to alanine mutation, yellow and red: hydrophobic to glutamic acid mutation, green: proline mutation. (E) TC544 (*gip1*Δ) cells were transformed with pRS424-GIP1-mutant-GFP coding for indicated mutants, sporulated for 24 h, and observed with DIC microscopy. Percentages of asci are shown in the diagram. More than 200 cells were observed in three independent colonies of each strain harboring indicated mutants (for a total of >600 cells). O/E: overexpression. In all images, scale bars indicate 5 μm.

between residues 358 and 476 contains a signal for nuclear localization. Localization of Gip1-N2 mutated in its helix2 also displayed a nuclear pattern. Thus, Gip1 must have multiple nuclear localization signals for postmeiotic nuclear localization. Therefore, we subjected the Gip1 sequence to NLS mapper, a software to search for nuclear localization signals, and found five putative NLSs (Figure 6A), in which the most N-terminal NLS overlaps with the N-terminal basic helix and the fourth NLS from the N-terminus (NLS1) lies between residues 358 and 476. Because the BM mutation disrupted the N-terminal NLS, we constructed Gip1-GFP carrying other mutations in combination; BN1: BM and NLS1M; BN2: BM, NLS1M, and NLS2M; BN3: BM, NLS1M, NLS2M, and NLS3M; BN4: BM, NLS1M, NLS2M, NLS3M, and NLS4M (Figure 6A). While Gip1-NLS1M and Gip1-BN1 localized to the nucleus in postmeiotic cells, Gip1-BN2, -BN3, and -BN4 showed the prospore membrane pattern (Figure 6B), suggesting that multiple NLSs contribute to the postmeiotic nuclear localization of Gip1.

To assess the physiological importance of Gip1 nuclear localization, cells carrying these different mutations were sporulated and spores were tested for the presence of the outermost dityrosine wall by detecting fluorescence of dityrosine. Because *DIT1* encoding an enzyme required for synthesis of dityrosine is expressed after closure of the prospore membrane (Briza *et al.*, 1990), and expression of *DIT1* fused to *lacZ* during spore formation is abolished when *GIP1* is deleted (Tachikawa *et al.*, 2001), we hypothesized that Gip1 regulates transcription of *DIT1* and formation of a dityrosine layer. However, although BN3 and BN4 showed weaker fluorescence and corresponding sporulation efficiency was decreased (Figure 6, C and D), all NLS mutants showed detectable dityrosine fluorescence and produced ethanol-resistant spores, indicating that spore walls are normal in these mutant cells (Figure 6E).

The third VXF sequence is the functional PP1-binding motif in Gip1, and Gip1 itself might be a target of PP1/Glc7

The PP1-binding motif valine-x-phenylalanine (VXF) is found in many targeting subunits of PP1/Glc7 and is required for their interaction with Glc7 and thus for function (Cannon, 2010). Gip1 has three VXF sequences (Figure 7A). These sequences were mutated (Gip1-G7M1–3) and a two-hybrid interaction analysis with Glc7 was performed. While Gip1-G7M1(V292A, F294A) and Gip1-G7M2(V446A, F448A) showed interaction with Glc7 at a level comparable to that of wild-type Gip1, Gip1-G7M3(V492A, F494A) did not interact with Glc7 (Figure 7B), suggesting that the third site is the functional PP1-binding motif. To confirm this, these Gip1 mutants were expressed as HA or GFP fusions in *gip1*Δ mutant cells and sporulated. Cells expressing Gip1-G7M1 and Gip1-G7M2 sporulated as well as those expressing wild-type Gip1. In contrast, cells expressing Gip1-G7M3 did not sporulate (Figure 7C) and showed a prospore membrane extension defect (Figure 7D bottom; see prospore membrane marker). Expression of Gip1-G7M3 was confirmed by Western blot (Figure 7E). These results demonstrate that the third PP1-binding motif (residues 492–494) is the functional PP1-binding motif of Gip1.

In the Western blot, we found that the band for Gip1-G7M3 was shifted to higher molecular weight (Figure 7E). Because Glc7 is a

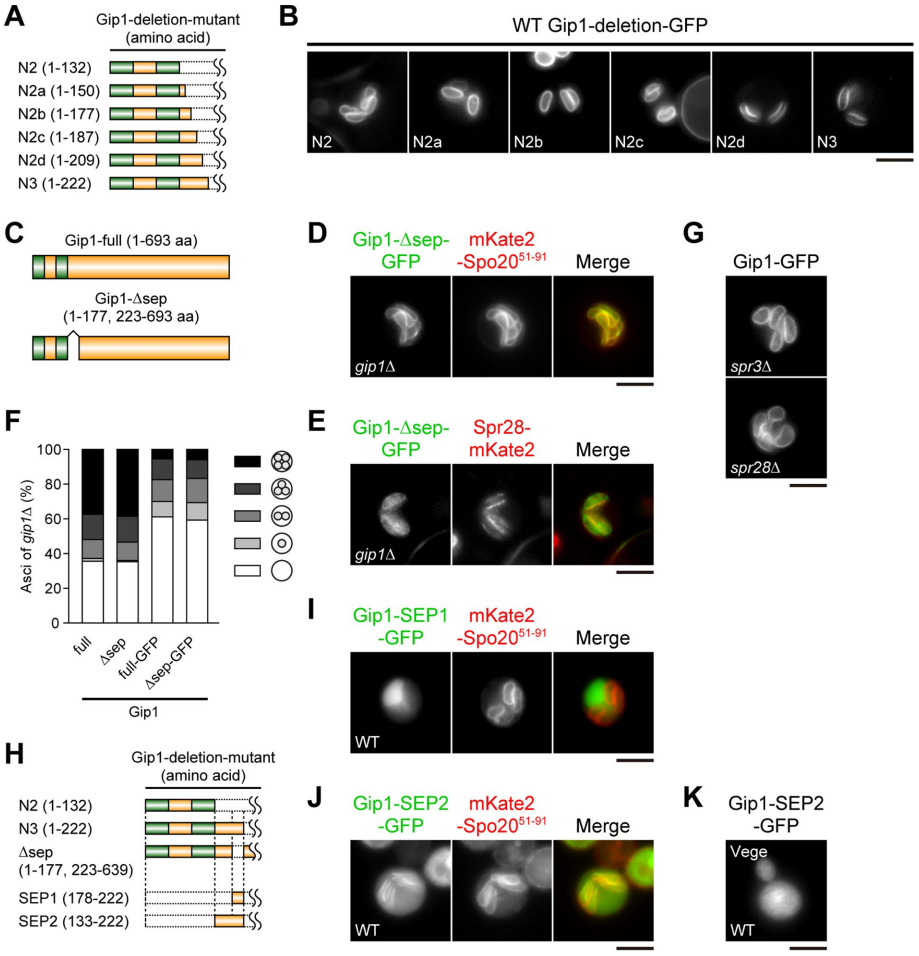

FIGURE 5: Analysis of Gip1 domains involved in its septin localization. (A) Schematic diagram of Gip1-N2-deletion-mutants are shown. Dark green: α-helix. (B) AN120 (wild-type) cells were transformed with pRS424-GIP1-N2-deletion-mutant-GFP, coding for indicated mutants, sporulated, and observed at 7–9 h. Representative cells are shown. (C) Schematic diagram of Gip1-Δsep mutants are shown. Dark green: α-helix. (D) TC544 (*gip1*Δ) cells were transformed with pRS424-GIP1-Δsep-GFP and pRS316-P_{TEF1}-mKate2-SPO20$^{51–91}$, sporulated, and observed at 7–9 h. Representative cells are shown. (E) TN300 (*gip1*Δ harboring integrated *SPR28-mKate2* and *mTagBFP2-SPO20*$^{51–91}$) cells were transformed with pRS424-GIP1-Δsep-GFP, sporulated, and observed at 7–9 h. Representative cells are shown. (F) TC544 (*gip1*Δ) cells were transformed with pRS314-GIP1 (full), pRS314-GIP1-Δsep (Δsep), pRS314-GIP1-GFP (full-GFP), or pRS314-GIP1-Δsep-GFP (Δsep-GFP), respectively, sporulated for 24 h, and observed with DIC microscopy. Percentages of asci are shown in the diagram. More than 200 cells were observed in three independent colonies of each strain harboring indicated mutants (for a total of >600 cells). O/E: overexpression. (G) NY528 (*spr3*Δ) and NY703 (*spr28*Δ) cells were transformed with pRS424-GIP1-Δsep-GFP, sporulated, and observed at 7–9 h. Representative cells are shown. (H) Schematic diagram of Gip1-SEP mutants are shown. Dark green: α-helix. (I, J) TNY375 (wild-type harboring integrated *mKate2-SPO20*$^{51–91}$) cells were transformed with pRS424-P_{TEF1}-GIP1-SEP1-GFP (I) or pRS424-P_{TEF1}-GIP1-SEP2-GFP (J), sporulated, and observed at 7–9 h. A representative cell is shown. (K) TNY375 (wild-type harboring integrated *mKate2-SPO20*$^{51-91}$) cells were transformed with pRS424-P^{TEF1}-GIP1-SEP2-GFP and observed under vegetative growing conditions. A representative cell is shown. In all images, scale bars indicate 5 μm.

phosphatase, this band shift might be caused by phosphorylation. Therefore, extracts of cells expressing Gip1 or Gip1-G7M3 were subjected to phosphatase treatment and analyzed. Both phosphatase-treated Gip1 and Gip1-G7M3 showed lower-molecular weight bands of the same size (Figure 7F). Thus, Gip1 is a phosphoprotein and Gip1-G7M3, which cannot interact with Glc7, is hyperphosphorylated, suggesting that Gip1 itself is a target of Glc7.

Interaction of Gip1 with PP1/Glc7 is required for its efficient release from the SPB during meiosis II and postmeiotic release from the prospore membrane

We also performed localization analysis of Gip1-G7M3 during sporulation. In *gip1*Δ cells, Gip1-G7M3 localized to small prospore membranes and SPBs, which was shown by colocalization with prospore membrane and SPB markers (Figure 7, D and G). In wild-type cells, Gip1-G7M3 localization mostly looked like wild-type Gip1 during meiosis, except that persistent SPB localization was more apparent (Figure 7, D and G). Together with the previous report that Glc7 partially localizes to SPB in *gip1*Δ cells (Tachikawa *et al.*, 2001), these observations indicate that Gip1 and Glc7 can localize to the SPB independently and suggest that complex formation may allow their efficient release from SPB.

In postmeiotic wild-type cells, Gip1-G7M3 remained on large prospore membranes and rarely translocated to the nucleus (Figure 7D). This indicates that the interaction of Gip1 with Glc7 is required for release of Gip1 from mature round prospore membranes. Consistent with this result, a large prospore membrane pattern instead of a nuclear pattern was observed in postmeiotic wild-type cells expressing Gip1-N2 to -N6, all of which lack this PP1-binding motif (Supplemental Figure S2).

Substitution of functions of Gip1 domains using chimeras

Our data suggest that the primary function of the Gip1 N-terminus is to recruit the protein to the prospore membrane and that the most important function of the Gip1 C-terminal domain is to bind to Glc7. To examine the former point, an alternative prospore membrane binding domain, GFP-Spo20$^{51–91}$, was fused to Gip1-C1 to -C3, and these chimeras were expressed in *gip1*Δ cells (Figure 8A). GFP-Spo20$^{51–91}$-Gip1-C1 to -C3 localized to the prospore membrane and GFP-Spo20$^{51–91}$-Gip1-C3 also localized to the septin bars during prospore membrane formation, as expected (Figure 8B). Cells expressing these proteins displayed ~50% sporulation, indicating that restoration of prospore membrane localization restores function (Figure 8C). These results indicate that the Gip1 N-terminus can be replaced by the prospore membrane localization signal of Spo20.

If the only function of Gip1 is to recruit Glc7 to the prospore membrane, Glc7 fused to a prospore membrane localization signal may bypass the requirement for Gip1. Thus, Glc7 was fused to GFP-Spo20$^{51–91}$, and this chimera was expressed in *gip1*Δ cells (Figure 8D). Although GFP-Spo20$^{51–91}$-Glc7 localized to the prospore

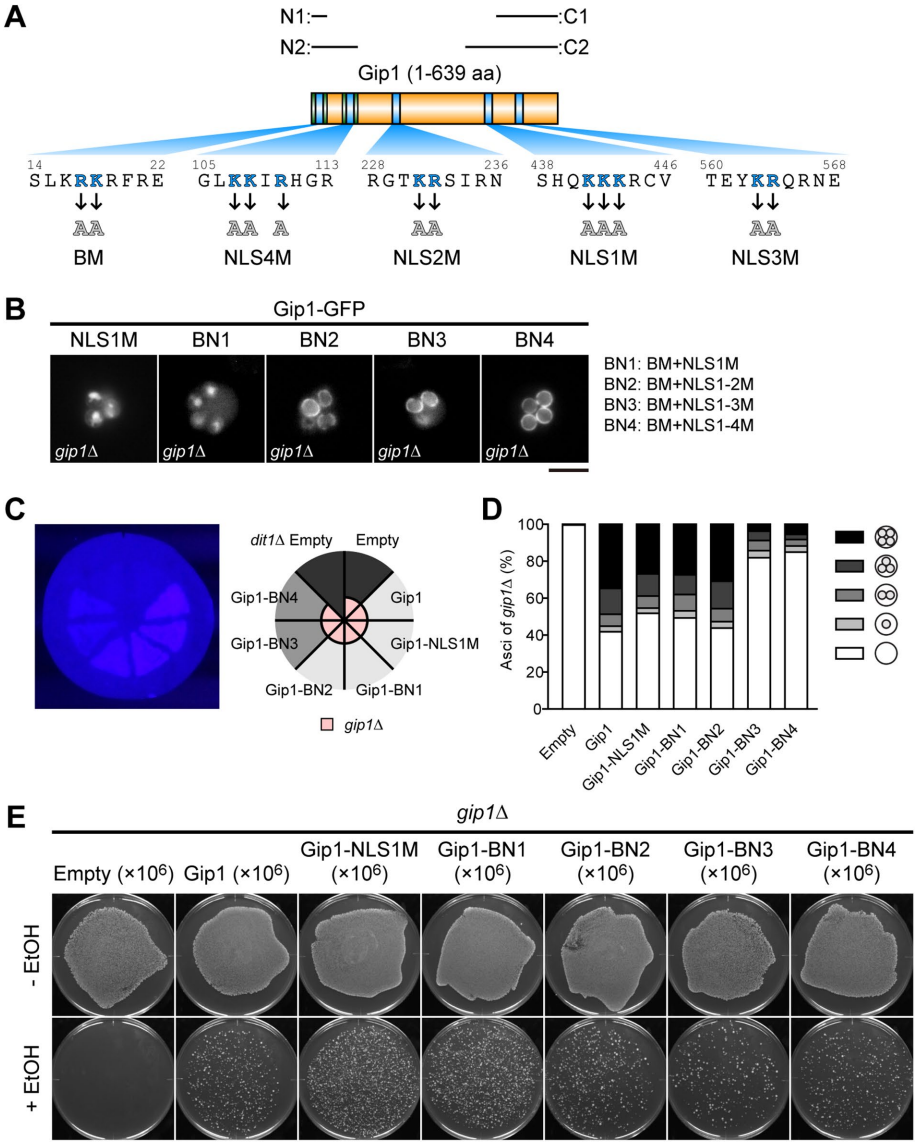

FIGURE 6: Analysis of the NLS of Gip1. (A) Schematic diagram of five putative NLSs of Gip1. N1, N2, C1, and C2 indicate the region of Gip1-deletion mutants. BM: basic residue mutation, NLS1M to NLS4M: NLS mutation. (B) TC544 (*gip1*Δ) cells were transformed with pRS424-GIP1-NLS-mutants-GFP, coding for indicated mutants, sporulated, and observed at 7–9 h. Representative cells are shown. BN1: BM+NLS1M; BN2: BM+NLS1–2M; BN3: BM+NLS1–3M; BN4: BM+NLS1–4M; Scale bar, 5 μm. (C) TC544 (*gip1*Δ) cells were transformed with pRS424-GIP1-NLS-mutants-GFP, coding for indicated mutants, or with empty vector, and AN264 (*dit1*Δ) cells were transformed with empty vector, cultured, and sporulated on filter paper for 2 d. This filter paper was treated with 10% ammonia solution and exposed to ultraviolet light. (D) TC544 (*gip1*Δ) cells were transformed with pRS424-GIP1-NLS-mutants-GFP, coding for indicated mutants, or with empty vector, sporulated for 24 h, and observed with DIC microscopy. The percentages of asci are shown in the diagram. More than 200 cells were observed in three independent colonies of each strain harboring indicated plasmids (for a total of >600 cells). (E) TC544 (*gip1*Δ) cells were transformed with pRS424-GIP1-NLS-mutants-GFP, coding for indicated mutants, or with empty vector, sporulated for 2 d. Samples of 1×10^6 cells of each transformant were treated with or without 26% ethanol and inoculated onto YPD plates for 2 d.

membrane as expected, and Gip1-C1-mCherry was slightly recruited to the membrane (Figure 8F). These results indicate that Glc7 recruited to the prospore membrane can only support sporulation in the presence of the Gip1 C-terminal region.

Gip1 may function in parallel to Spo73, Spo71, and Vps13

The prospore membrane extension defect of the *gip1*Δ mutant is similar to that seen in the *spo73*Δ, *spo71*Δ, and *vps13*Δ mutants. However, phenotypes of these mutants are distinct in some regards. While intraluminal vesicles are observed between inner and outer leaflets of the prospore membrane in *spo73*Δ, *spo71*Δ, and *vps13*Δ cells (Park and Neiman, 2012; Park *et al.*, 2013; Okumura *et al.*, 2016), no such structures were observed in *gip1*Δ cells (Tachikawa *et al.*, 2001). Prospore membrane closure is partially defective in *spo73*Δ, *spo71*Δ, and *vps13*Δ cells; in contrast, prospore membrane closure is normal in *gip1*Δ cells (Park and Neiman, 2012). While nuclear capture by the prospore membrane is partially defective in *spo73*Δ, *spo71*Δ, and *vps13*Δ cells (Okumura *et al.*, 2016), our observations showed that nuclear capture is normal in *gip1*Δ cells.

To examine the relationship between *GIP1* and *SPO73*, *SPO71*, or *VPS13*, genetic interactions and localization dependencies were examined. First, GFP-Spo73, Spo71-GFP, and Vps13-GFP were overexpressed in *gip1*Δ cells during sporulation. GFP-Spo73 and Spo71-GFP localized on the prospore membrane in *gip1*Δ cells (Figure 9A). No suppression of the sporulation defect was observed, although larger prospore membranes were observed in 2.5% of the cells overexpressing GFP-Spo73 and 30% of the cells overexpressing Spo71-GFP (Figure 9A). For Vps13-GFP, a clear localization pattern was not observed even in wild-type cells (unpublished data), probably because of overexpression. When genomic *VPS13* was tagged with GFP in the *gip1*Δ mutant, localization to the prospore membrane was observed (Figure 9B). A *gip1* temperature-sensitive allele was also examined for suppression by overexpression of GFP-Spo73, Spo71-GFP, and Vps13-GFP, but again, no suppression was observed (unpublished data). These results indicate that overexpression of Spo73, Spo71, and Vps13 cannot suppress *gip1*Δ and that localization of Spo73, Spo71, and Vps13 is not dependent on Gip1.

membrane, it could not rescue the sporulation defect of the *gip1*Δ mutant. However, when this chimera was coexpressed with Gip1-C1, which contains a functional PP1-binding motif, but does not contain a prospore membrane localization signal, the sporulation defect was significantly rescued (16% sporulation) (Figure 8E). In these cells, GFP-Spo20$^{51–91}$-Glc7 localized on the prospore

Conversely, Gip1-GFP was overexpressed in *spo73*Δ, *spo71*Δ, and *vps13*Δ cells. No sporulation was observed, and localization of Gip1-GFP to the prospore membrane appeared normal (Figure 9C). A fraction of cells displayed a narrow extending prospore membrane

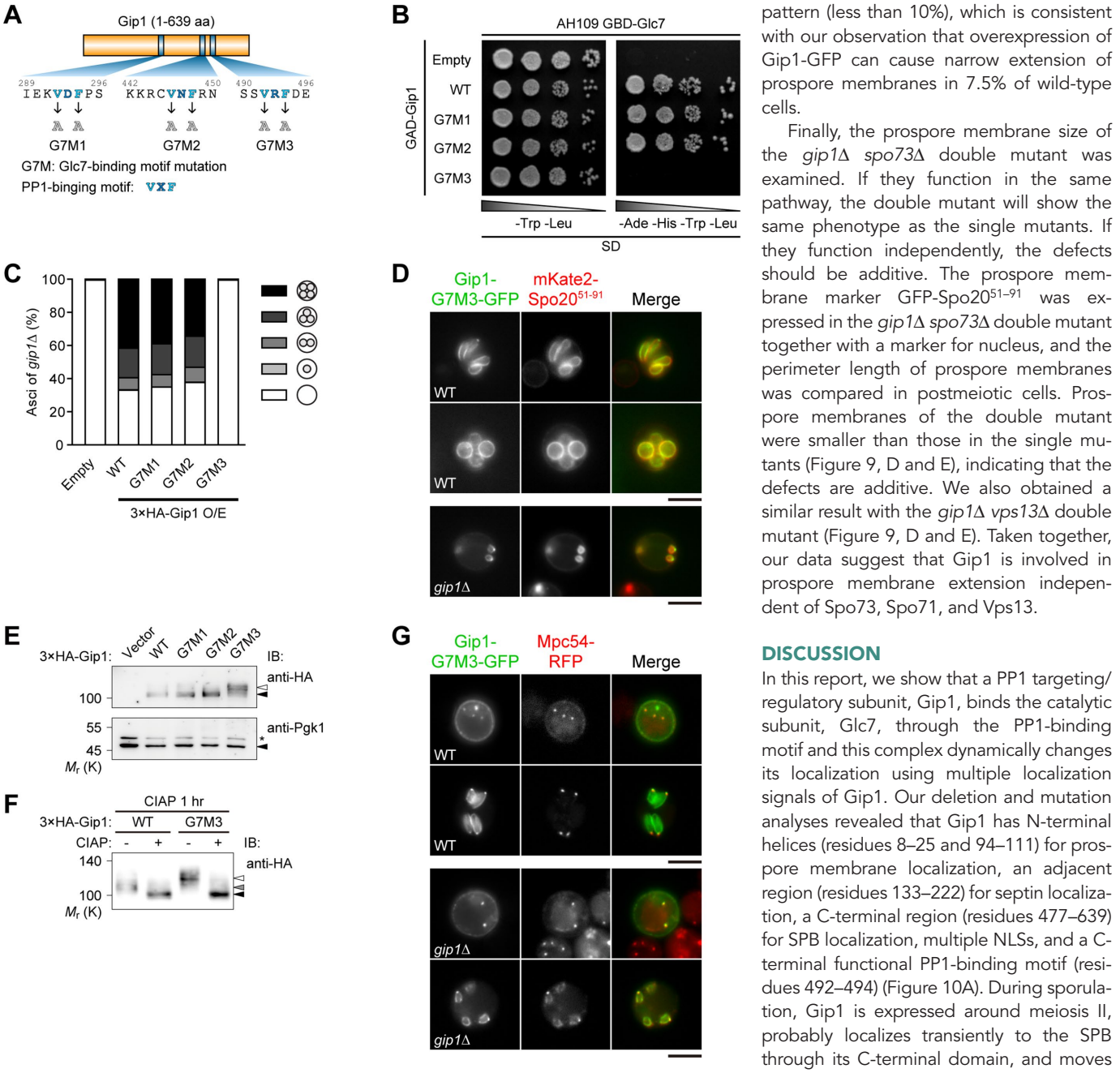

FIGURE 7: Analysis of the interaction between Gip1 and Glc7. (A) Schematic diagram of Gip1-G7M mutants is shown. G7M: Glc7 binding mutation; dark blue: PP1-binding motif [VXF]. (B) AH109 cells were transformed with pGBKT7-GLC7 and pGADT7-GIP1-wild type/mutants or empty vector, cultured, and 10-fold serial dilutions were spotted onto indicated SD plates. Each plate was incubated 2 d at 30°C. (C) TC544 (*gip1*Δ) cells were transformed with pRS426-P_{SPO20}-3×HA-GIP1-wild type/G7M-mutants or empty vector, sporulated for 24 h, and observed with DIC microscopy. Percentages of asci are shown in the diagram. More than 200 cells were observed in three independent colonies of each strain harboring indicated mutants (for a total of >600 cells). O/E: overexpression. (D) AN120 (wild-type) and TC544 (*gip1*Δ) cells were transformed with pRS424-GIP1-G7M3-GFP and pRS316-P_{TEF1}-mKate2-SPO20$^{51–91}$, sporulated, and observed at 7–9 h. Representative cells are shown. (E) TC544 (*gip1*Δ) cells were transformed with pRS426-P_{SPO20}-3×HA-GIP1-wild type/G7M-mutants or empty vector, sporulated, and lysed. Proteins were then probed by Western blotting using anti-HA, with anti-Pgk1 as internal control. Top, Open arrowhead: a major band of 3×HA-Gip1-G7M3; closed arrowhead: major bands of 3×HA-Gip1 and 3×HA-Gip1-G7M1 and -G7M2 mutants. Bottom, Closed arrowhead: bands for Pgk1; asterisk: nonspecific bands. (F) TC544 (*gip1*Δ) cells were transformed with pRS426-P_{SPO20}-3×HA-GIP1 or pRS426-P_{SPO20}-3×HA-GIP1-G7M3-mutant, sporulated, and lysed. TCA-treated samples were then treated with or without CIAP and proteins were probed by Western blotting using anti-HA. Open arrowhead: 3×HA-Gip1-G7M3; closed arrowhead: lower-shifted 3×HA-Gip1 and 3×HA-Gip1-G7M3. (G) TNY293 (wild-type harboring integrated *MPC54-RFP* and *mTagBFP2-SPO20*$^{51–91}$) and TNY294 (*gip1*Δ harboring integrated *MPC54-RFP* and *mTagBFP2-SPO20*$^{51–91}$) cells were transformed with pRS424-GIP1-G7M3-GFP, sporulated, and observed at 7–9 h. Representative cells are shown. In all images, scale bars indicate 5 μm.

pattern (less than 10%), which is consistent with our observation that overexpression of Gip1-GFP can cause narrow extension of prospore membranes in 7.5% of wild-type cells.

Finally, the prospore membrane size of the *gip1*Δ *spo73*Δ double mutant was examined. If they function in the same pathway, the double mutant will show the same phenotype as the single mutants. If they function independently, the defects should be additive. The prospore membrane marker GFP-Spo20$^{51–91}$ was expressed in the *gip1*Δ *spo73*Δ double mutant together with a marker for nucleus, and the perimeter length of prospore membranes was compared in postmeiotic cells. Prospore membranes of the double mutant were smaller than those in the single mutants (Figure 9, D and E), indicating that the defects are additive. We also obtained a similar result with the *gip1*Δ *vps13*Δ double mutant (Figure 9, D and E). Taken together, our data suggest that Gip1 is involved in prospore membrane extension independent of Spo73, Spo71, and Vps13.

DISCUSSION

In this report, we show that a PP1 targeting/regulatory subunit, Gip1, binds the catalytic subunit, Glc7, through the PP1-binding motif and this complex dynamically changes its localization using multiple localization signals of Gip1. Our deletion and mutation analyses revealed that Gip1 has N-terminal helices (residues 8–25 and 94–111) for prospore membrane localization, an adjacent region (residues 133–222) for septin localization, a C-terminal region (residues 477–639) for SPB localization, multiple NLSs, and a C-terminal functional PP1-binding motif (residues 492–494) (Figure 10A). During sporulation, Gip1 is expressed around meiosis II, probably localizes transiently to the SPB through its C-terminal domain, and moves on to the newly formed prospore membrane through two helices in the N-terminal domain (Figure 10B). Through the region following the N-terminal helices, Gip1 then

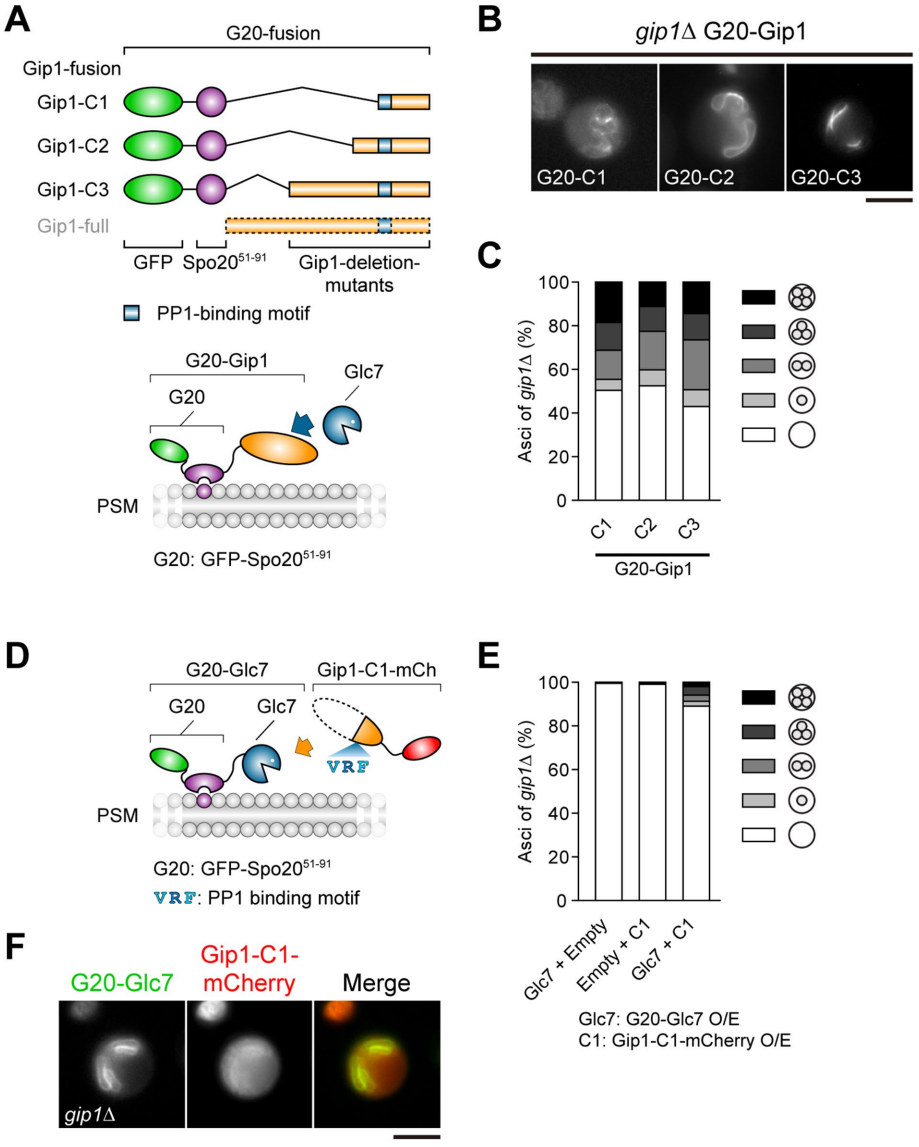

FIGURE 8: Analysis of the function of prospore membrane-targeted Gip1 and Glc7. (A) Schematic diagram of G20-fused Gip1 mutants is shown. G20: GFP-Spo20$^{51–91}$; green: GFP; purple: Spo20$^{51–91}$ and phosphatidic acid (bottom panel); dark blue box: PP1-binding motif (VRF). (B) TC544 (*gip1*Δ) cells were transformed with pRS424-P$_{SPR3}$-GFP-SPO20$^{51–91}$-GIP1-mutants (G20-Gip1), coding for indicated mutants, sporulated, and observed at 7–9 h. Representative cells are shown. (C) TC544 (*gip1*Δ) cells were transformed with pRS424-P$_{SPR3}$-GFP-SPO20$^{51–91}$-GIP1-mutants (G20-Gip1), coding for indicated mutants, sporulated for 24 h, and observed with DIC microscopy. Percentages of asci are shown in the diagram. More than 200 cells were observed in three independent colonies of each strain harboring indicated deletion mutants (for a total of >600 cells). (D) Schematic diagram of coexpression of G20-fused Glc7 and Gip1-C1 mutant are shown. G20: GFP-Spo20$^{51–91}$; VRF: PP1-binding motif. (E) TC544 (*gip1*Δ) cells were transformed with pRS424-P$_{SPR3}$-GFP-SPO20$^{51–91}$-GLC7-mutant (G20-Glc7 O/E) or pRS424 (empty vector), and pRS426-GIP1-C1-mCherry (Gip1-C1-mCherry O/E) or pRS426 (empty vector), respectively. All transformants were sporulated for 24 h and observed with DIC microscopy. The percentages of asci are shown in the diagram. More than 200 cells were observed in three independent colonies of each strain harboring indicated plasmids (for a total of >600 cells). O/E: overexpression. (F) TC544 (*gip1*Δ) cells were transformed with pRS424-P$_{SPR3}$-GFP-SPO20$^{51–91}$-GLC7 mutant (G20-Glc7 O/E) and pRS426-GIP1-C1-mCherry, sporulated, and observed at 7–9 h. A representative cell is shown. In all images, scale bars indicate 5 μm.

colocalizes with septins, which form bars along the prospore membrane. After closure of the prospore membrane, Gip1 spreads transiently around the prospore membrane and then translocates to the nucleus, dependent on its multiple NLSs. Further, a mutation in the PP1-binding motif of Gip1 altered its localization, indicating that dynamic localization of the targeting subunit, Gip1, is also dependent on its interaction with the catalytic subunit through this motif.

This report also describes involvement of the Gip1–Glc7 complex in prospore membrane formation during sporulation. The *gip1*Δ mutant was shown to form only small prospore membranes; thus, Gip1 is required for prospore membrane extension. Our genetic analysis also revealed that Gip1–Glc7 functions independently of Spo73, Spo71, and Vps13, which function together on the prospore membrane in its extension, possibly through lipid regulation (Parodi *et al.*, 2015; Okumura *et al.*, 2016; Park *et al.*, 2016). This is consistent with phenotypic difference between the mutants; while nuclear capture by the prospore membrane was partially defective, intraluminal vesicles are observed, and closure of the prospore membrane was partially defective in *spo73*Δ, *spo71*Δ, and *vps13*Δ mutants (Park and Neiman, 2012; Park *et al.*, 2013; Okumura *et al.*, 2016), nuclear capture was normal, no intraluminal vesicles were observed (Tachikawa *et al.*, 2001), and closure of prospore membranes was normal in the *gip1*Δ mutant (Park and Neiman, 2012). We suggest that Gip1–Glc7 functions in a novel pathway contributing prospore membrane extension.

Gip1 colocalizes with septins and is required for proper septin organization along the prospore membrane (Tachikawa *et al.*, 2001); however, colocalization of Gip1 with the septin bars was not required for proper septin organization. Rather, localization of Gip1 to the prospore membrane was sufficient to promote septin organization. This suggests that Gip1–Glc7 phosphatase may target proteins on the prospore membrane whose dephosphorylation is important for subsequent septin organization. This idea is consistent with the reported assembly of septin complexes by diffusion-driven annealing on membranes (Bridges *et al.*, 2014). Recently, it was reported that septins are required for prospore membrane morphogenesis using strains of different background from SK1 (Heasley and McMurray, 2016). In our SK1 background strains, we can only see modest sporulation defects in the septin mutants (unpublished observation). In this same background strain, *gip1*Δ mutants fail to sporulate and completely arrest with small prospore membranes. Thus, although septin organization is regulated by Gip1–Glc7, the sporulation defect of *gip1*Δ cells cannot be explained by regulation of septin structures.

The region of Gip1 necessary and sufficient for association with the septins along the prospore membrane did not localize to

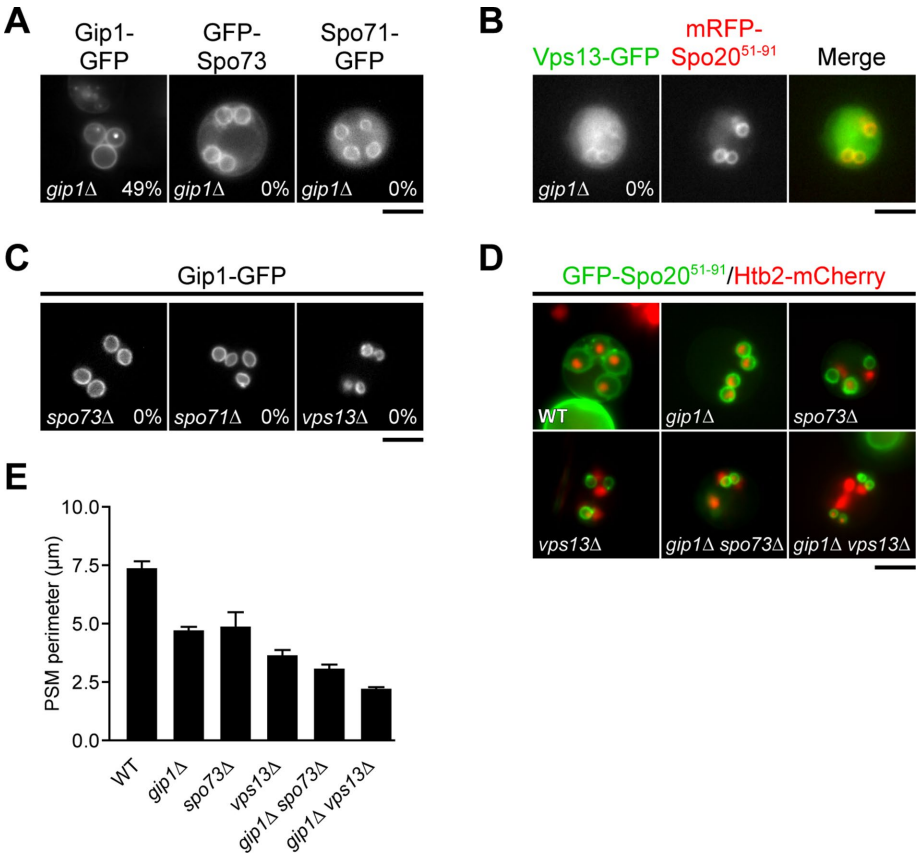

FIGURE 9: Genetic interaction among *GIP1*, *SPO73*, *SPO71*, and *VPS13*. (A) TC544 (*gip1*Δ) cells were transformed with pRS424-GIP1-GFP, pRS424-P_{SPO20}-GFP-SPO73, or pRS424-SPO71-GFP, sporulated for 7–9 h, subjected to fluorescence microscopy, and observed at 24 h with DIC microscopy. Representative cells are shown. Bottom numbers indicate sporulation efficiency, the percentage of cells that formed at least one spore. (B) HJY65 (*gip1*Δ *VPS13-GFP*) cells were transformed with pRS426-P_{TEF1}-mRFP-SPO20$^{51–91}$, sporulated, and observed at 7–9 h. Bottom number indicates sporulation efficiency when *VPS13-GFP* was overexpressed (for a total of >600 cells). A representative cell is shown. (C) TC545 (*spo73*Δ), TC581 (*spo71*Δ), and TC572 (*vps13*Δ) cells were transformed with pRS424-GIP1-GFP, sporulated for 7–9 h, subjected to fluorescence microscopy, and observed at 24 h with DIC microscopy. Representative cells are shown. Bottom number indicates sporulation efficiency (for a total of >600 cells). (D) AN120 (wild-type), TC544 (*gip1*Δ), TC545 (*spo73*Δ), TC572 (*vps13*Δ), TC564 (*gip1*Δ *spo73*Δ), and TNY411 (*gip1*Δ *vps13*Δ) cells were transformed with pRS424-P_{TEF1}-GFP-SPO20$^{51–91}$ and pRS316-HTB2-mCherry, sporulated, and observed at 7–9 h. A representative cell is shown. (E) Prospore membrane perimeters of postmeiotic cells of strains AN120 (wild-type), TC544 (*gip1*Δ), TC545 (*spo73*Δ), TC572 (*vps13*Δ), TC564 (*gip1*Δ *spo73*Δ), and TNY411 (*gip1*Δ *vps13*Δ) are shown as the mean ± the SD. More than 50 PSMs were examined in three independent colonies of each strain. The data of WT and *gip1*Δ are the same as in Figure 1C. $P < 0.05$ (*gip1*Δ–*vps13*Δ, *spo73*Δ–*vps13*Δ); $P < 0.01$ (*vps13*Δ–[*gip1*Δ *vps13*Δ]); $P < 0.001$ (WT–*gip1*Δ, WT–*spo73*Δ, WT–*vps13*Δ, WT–[*gip1*Δ *spo73*Δ], WT–[*gip1*Δ *vps13*Δ], *gip1*Δ–[*gip1*Δ *spo73*Δ], *spo73*Δ–[*gip1*Δ *spo73*Δ], *gip1*Δ–[*gip1*Δ *vps13*Δ], *vps13*Δ–[*gip1*Δ *vps13*Δ], and *spo73*Δ–[*gip1*Δ *vps13*Δ]) (Tukey–Kramer test). In all images, scale bars indicate 5 μm.

septin structures at the bud neck when expressed in vegetative cells. During sporulation, septin filaments have components different from that in vegetative cells; two subunits, Spr3 and Spr28, replace Cdc12 and Cdc11/Shs1, and thus have distinct properties (Garcia *et al.*, 2016). Thus, the septin localization signal may be specific for the sporulation-specific septins. Consistent with the idea that septin-association sequences might be different in vegetative and sporulating cells, a previous study found that the vast majority of septin-associated proteins in vegetative cells fail to associate with the septin bars during sporulation (Lam *et al.*, 2014). In addition, although we compared the sequence of Gip1-SEP2 (residues 133–222) with those in previously reported septin-binding proteins, including Bni5 (Finnigan *et al.*, 2015), Bud4 (residues 623–774; Wu *et al.*, 2015), Hsl1 (residues 611–950; Finnigan *et al.*, 2016) and Hof1 (residues 293–355; Meitinger *et al.*, 2013), apparently related sequences could not be found. Further analysis to define the septin localization sequences in Gip1 will identify a sporulation-specific septin localization signal and may contribute to the understanding of structural differences between septin structures in vegetative and sporulating cells.

We showed that postmeiotic localization of Gip1 to the nucleus is dependent on multiple NLSs. Considering that Gip1 is required for expression of Dit1 in postmeiotic cells (Tachikawa *et al.*, 2001), we expected to see spore wall defects when NLS mutants were expressed as a sole *GIP1* allele. However, no spore wall defect was observed. Taken together with our result from time-lapse analysis, in which Gip1 disappears quickly in the nucleus, postmeiotic nuclear localization of Gip1 does not appear to be necessary for transcriptional induction of later meiotic genes, but rather may contribute to efficient degradation of the protein, which could allow reuse of Glc7.

Gip1 binds PP1/Glc7 through the PP1-binding motif located in its C-terminal region, and a Gip1 protein carrying a mutation in this motif was nonfunctional and hyperphosphorylated. There are reports showing that some targeting subunits are dephosphorylated by Glc7 (Sanz *et al.*, 2000; Gardiner *et al.*, 2007; Akiyoshi *et al.*, 2009), and our results suggest that the Glc7-targeting subunit Gip1 is itself one of the targets of Glc7. Analysis of the localization of Gip1 mutant protein defective in binding to Glc7 in *gip1*Δ cells showed that this mutant protein is not efficiently released from the SPB. In cells where wild-type Gip1 is also present, the mutant protein is eventually released from the SPB, but then remains on the prospore membrane after closure and does not translocate to the nucleus. These observations suggest that dephosphorylation by Glc7 may be required for efficient release of Gip1 both from the SPB upon the initiation of prospore membrane formation and from the prospore membrane after closure. However, we cannot rule out the possibility that interaction of Gip1 with PP1/Glc7 is important and phosphorylation status of Gip1 is secondary effect caused by physical interference of phosphorylation.

When Glc7 was ectopically targeted to the prospore membrane independent of *GIP1* by the fusion with Spo20$^{51–91}$, this was not sufficient to rescue a *gip1*Δ; however, coexpression of the membrane targeted Glc7 with a C-terminal fragment of Gip1 containing PP1-binding motif did restore sporulation. This suggests that, while the N-terminal region of Gip1 functions in targeting the Gip1–Glc7

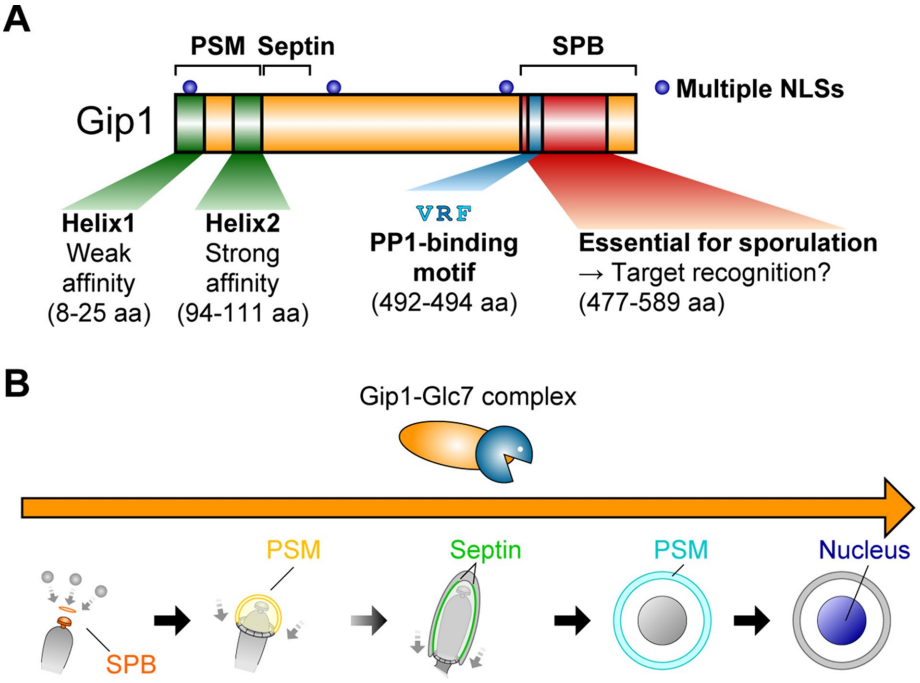

FIGURE 10: Contribution of Gip1 domains to its multiple localization and function during sporulation. (A) Domains of Gip1. In the N-terminal region, two α-helices contribute to prospore membrane localization of Gip1 and a region adjacent to the C-terminus of helix2 is essential for septin localization of Gip1. Multiple NLSs contribute to nuclear localization of Gip1, although the physiological importance of nuclear localization is unclear. In the C-terminal region, residues 477–639 contribute to SPB localization of Gip1, and Gip1 binds Glc7 through PP1-binding motif at residues 492–494. Besides the interaction with the SPB and Glc7, the C-terminal region may also be required for recognition of a critical PP1 phosphatase target(s). (B) Dynamic change of the localization of the Gip1–Glc7 complex during prospore membrane formation. Initially, the Gip1–Glc7 complex probably localizes transiently to the SPB and moves onto the prospore membrane. As the prospore membrane extends, the Gip1–Glc7 complex colocalizes with septins. After closure of the prospore membrane, the Gip1–Glc7 complex transiently spreads around the prospore membrane and then translocates into the nucleus.

phosphatase complex to the prospore membrane, the C-terminal region contributes not only to binding to Glc7 but also to substrate recognition by the phosphatase complex.

We still do not know the target of Gip1–Glc7 phosphatase essential for prospore membrane extension. The defect in membrane extension in *gip1*Δ could be a result of a defect in vesicle fusion at the prospore membrane. Possible targets for Gip1–Glc7 are the SNARE proteins involved in this fusion event and its upstream regulators such as Sec4, Sec2, and exocyst components. It is reported that Glc7 is involved in the final stage of SNARE-mediated vesicle fusion in yeast vesicular transport in vegetative cells (Peters *et al.*, 1999; Bryant and James, 2003). It is also reported that SNAP-25 is regulated by phosphorylation and its dephosphorylation is dependent on PP1 in PC12 cells (Gao *et al.*, 2012). During prospore membrane formation, a development-specific SNARE, Spo20, is expressed and functions with Sso1 and Snc1/2 (Neiman *et al.*, 2000). This sporulation-specific SNARE complex could be responsible for the prospore membrane extension defect of *gip1*Δ. It is also possible that the LEC is a responsible target. In this case, premature closure of the prospore membrane could occur, which causes the prospore membrane extension defect of *gip1*Δ. We have data suggesting an interaction between a Gip1-interacting protein, Ysw1, and the LEC (unpublished observation).

PP1 and its targeting/regulatory subunits have been extensively studied (Bollen *et al.*, 2010; Cannon, 2010). Among PP1-targeting subunits, Gip1 appears to be one of the most dynamic, responsible for moving the PP1 complex through different localizations in coordination with the events of sporulation. Further study to identify the targets of Gip1–Glc7 will provide an excellent model for regulation of PP1 during a developmental process.

MATERIALS AND METHODS

Yeast strains and media

Standard media and genetic techniques were used unless otherwise noted (Adams *et al.*, 1997). All yeast strains used in this study, which were derived from the SK1 background, are listed in Supplemental Table 1. PCR-based gene alterations were performed as previously described (Longtine *et al.*, 1998). Strains were constructed with the primers and plasmids in Supplemental Tables 2 and 3. In brief, HJY65: IC4, IC5, pFA6a-yEGFP-HIS3MX6; TC134: TN281, TN282, pFA6a-yEGFP-HIS3MX6; TC544: HT282, HT309, pFA6a-kanMX6; TC564: IC7, IC8, genome of TC555; TNY293 and TNY294: mod_pRS303-P_{TEF1}-mTagBFP2-SPO20$^{51–91}$ and pRS306-MPC54-RFP; TNY299: mod_pRS303-P_{TEF1}-mTagBFP2-SPO20$^{51–91}$ and pRS306-SPR28-mKate2; TNY375: mod_pRS303-P_{TEF1}-mKate2-SPO20$^{51–91}$; TNY411: TN433, TN434, genome of HI29. All PCR-based integrations and disruptions were confirmed by genomic PCR. All of the deletions constructed in this study were confirmed to be rescuable by expression of the deleted genes.

Plasmids

The plasmids used in this study are listed in Supplemental Table 3 in the Supplemental Materials. To generate mod_pRS303, an *HIS3* endogenous *Kpn*I site-eliminated variant, FRP467 (Addgene), was digested with *Nhe*I and *Sac*I, and the HIS3 fragment was cloned into pRS303 (Sikorski and Hieter, 1989).

pRS316-P_{TEF1}-mKate2-SPO20$^{51–91}$ was generated as follows: First, the P_{TEF1} fragment was amplified with TN25 and TN26 and with pRS424-P_{TEF1}-GFP-SPO20$^{51–91}$ (Nakanishi *et al.*, 2004) as a template, digested with *Sac*I and *Not*I, and cloned into pRS316 (Sikorski and Hieter, 1989) to generate pRS316-P_{TEF1}. Second, the *mKate2* fragment was synthesized by gBlocks (Integrated DNA Technologies: IDT), amplified with TN357 and TN358, and digested with *Not*I and *Xba*I, and the *SPO20*$^{51–91}$-T_{CYC1} fragment was cut out from pRS424-P_{TEF1}-GFP-SPO20$^{51–91}$ with *Xba*I and *Kpn*I. Then both fragments were cloned into pRS316-P_{TEF1}. mod_pRS303-P_{TEF1}-mTagBFP2-SPO20$^{51–91}$ was generated as follows: First, P_{TEF1}-*mKate2-SPO20*$^{51–91}$ was cloned into mod_pRS303. Second, the *mTagBFP2* fragment was synthesized by gBlocks (IDT), amplified with TN408 and TN409, digested with *Not*I and *Bam*HI, and cloned into *Not*I–*Bgl*II digested mod_pRS303-P_{TEF1}-mkate2-SPO20$^{51–91}$. To construct pRS306-MPC54-RFP, the *MPC54-RFP* fragment was cut out from pRS316-MPC54-RFP (Mathieson *et al.*, 2010) with *Kpn*I and *Sac*I and cloned into pRS306 (Sikorski and Hieter, 1989). pRS316-SPR28-mKate2 was generated as follows: First, the *mCherry* fragment was

amplified with TN98 and TN99 using pFA6a-mCherry-HIS3MX6 (gift from M. Onishi, Stanford University School of Medicine) as a template, digested with *Xho*I and *Kpn*I, and cloned into pRS316-P_{TEF1}. Second, the *mKate2* fragment was amplified with TN380 and TN381, digested with *Pac*I and *Asc*I, and cloned into pRS316-P_{TEF1}-C-mCherry. Finally, the *SPR28* fragment was amplified with TN175 and TN176, digested with *Sac*I and *Eco*RI, and cloned into pRS316-P_{TEF1}-C-mKate2. To construct pRS306-SPR28-mKate2, the *SPR28-mKate2* fragment was cut out from pRS316-SPR28-mKate2 with *Sac*I and *Kpn*I and cloned into pRS306. To generate pRS316-NOP1-mCherry, the *NOP1* fragment was amplified with TN503 and YO325, digested with *Sac*I and *Xho*I, and cloned into pRS316-P_{TEF1}-C-mCherry. pRS424-GIP1-GFP was generated as follows: First, the chromosomal copy of *GIP1* was fused to *GFP* using HT281, HT282, and pFA6a-yEGFP-HIS3MX6 (Nickas and Neiman, 2002) as a template and created TC134 strain. Second, the *GIP1-GFP* fragment was amplified with HT66 and HT84, digested with *Xho*I and *Sac*II, and cloned into pRS316. Finally, the *GIP1-GFP* fragment was cut from pRS316-GIP1-GFP and cloned into pRS424 (Christianson *et al.*, 1992).

To generate the GIP1-deletion mutant series, pRS424-GIP1-(N1 to N8, and C1 to C3)-GFP, each liner fragment was amplified by inverse PCR using indicated primers and pRS424-GIP1-GFP as a template and digested with *Not*I or *Cla*I, followed by self-ligation. To introduce Gip1 N-terminal mutations, BM, HyM, HeM1, HeM2, each liner fragment was amplified using indicated primers and templates, followed by self-ligation. To generate pRS424-GIP1-(N2a to N2d), each liner fragment was amplified by inverse PCR using indicated primers and pRS424-GIP1-N3-GFP as a template and digested with *Cla*I, followed by self-ligation. pRS314-GIP1-Δsep was generated as follows: First, *GIP1* N-terminal fragment was cut out from pRS424-GIP1-GFP with *Xho*I and *Eco*RI, *GIP1* C-terminal fragment was cut out from pRS306-GIP1 with *Eco*RI and *Sac*II, and both were cloned into pRS314 (Sikorski and Hieter, 1989) to generate pRS314-GIP1. Second, the pRS314–GIP1–Δsep liner fragment was amplified by inverse PCR using indicated primers and templates and digested with *Cla*I, followed by self-ligation. To generate pRS424–GIP1–Δsep–GFP, a liner fragment was amplified by inverse PCR with YN69 and YN128, and with pRS424-GIP1-GFP as a template, and digested with *Cla*I, followed by self-ligation. To generate pRS314-GIP1-Δsep-GFP, *GIP1-Δsep* fragment was cut out from pRS424-GIP1-Δsep-GFP with *Kpn*I and *Pac*I and cloned into pRS424-GIP1-GFP. pRS424-P_{TEF1}-GIP1-SEP1-GFP was generated as follows: First, the *GFP-*T_{ADH1} fragment was amplified using YSMO017 and YSMO018, with pFA6a-GFP(S65T)-HIS3MX6 as a template, digested with *Xho*I and *Kpn*I, and cloned into pRS424-P_{TEF1} to generate pRS424-P_{TEF1}-C-GFP-T_{ADH1}. Second, the *GIP1-SEP1* fragment was amplified using TN507 and TN508, digested with *Eco*RI and *Xho*I, and cloned into pRS424-P_{TEF1}-C-GFP-T_{ADH1}. To generate pRS424-P_{TEF1}-GIP1-SEP1-GFP, the *GIP1-SEP2* fragment was amplified using TN508 and TN578, digested with *Bam*HI and *Xho*I, and cloned into pRS424-P_{TEF1}-C-GFP-T_{ADH1}.

To introduce Gip1-NLS mutations, BM, NLS1-4M, each liner fragment was amplified using indicated primers and templates, followed by self-ligation.

pRS426-P_{SPO20}-3×HA-GIP1-(G7M1 to G7M3) were generated as follows: First, the *GIP1* C-terminal fragment was cut out from pRS306-GIP1 with *Sal*I and *Sac*II and cloned into pRS306 to generate pRS306-GIP1-C. Second, the *P_{SPO20}-3×HA-GIP1* N-terminal fragment was cut out from pSB5 (Tachikawa *et al.*, 2001) with *Sal*I, cloned into pRS306-GIP1-C to generate pRS306-P_{SPO20}-3×HA-GIP1. Third, the *P_{SPO20}-3×HA-GIP1* fragment was cut from pRS306-P_{SPO20}-3×HA-GIP1 with *Kpn*I and *Sac*II and cloned into pRS426 (Christianson *et al.*, 1992) to generate pRS426-P_{SPO20}-3×HA-GIP1. Finally, pRS426-P_{SPO20}-3×HA-GIP1-(G7M1 to G7M3) liner fragments were amplified by inverse PCR using indicated primers and pRS426-P_{SPO20}-3×HA-GIP1 as a template, followed by self-ligation. To generate pGADT7-GIP1 and G7M1 to G7M3 mutants, each fragment was amplified with HT315 and YSO319, and indicated templates, digested with *Bam*HI and *Xho*I using the internal *Bam*HI site, and cloned into pGADT7 (Clontech). To construct pRS424-GIP1-G7M3-GFP, the *GIP1* N-terminal fragment was cut out from pRS424-GIP1-GFP with *Xho*I and *Bgl*II, the *GIP-G7M3* C-terminal fragment was cut out from pRS426-P_{SPO20}-3×HA-GIP1-G7M3 with *Bgl*II and *Eco*RI, and both were cloned into *Xho*I- and *Eco*RI-digested pRS424-GIP1-C1-GFP. To construct pRS424-GIP1-C1-G7M3-GFP, the *GIP-C1–G7M3* fragment was amplified with YN12 and pRS-R using pRS424-GIP1-G7M3-GFP as a template and digested with *Not*I and *Sac*I, the *GIP1* promotor fragment was cut out from pRS424-GIP1-C1-GFP with *Kpn*I and *Not*I, and both were cloned into *Kpn*I- and *Sac*I-digested pRS424. To generate pGBKT7-GLC7, the *GLC7* fragment was amplified with YO322 and YO325, digested with *Nco*I and *Pst*I, and cloned into GBKT7 (Clontech).

pRS424-P_{SPR3}-GFP-SPO20$^{51–91}$-GIP1-C1 to C3 was generated as follows: First, the *T_{CYC1}* fragment was cut out from pRS424-P_{TEF1}-GFP-SPO20$^{51–91}$ with *Xho*I and *Kpn*I and cloned into pRS424 to generate pRS424-T_{CYC1}. Second, the *P_{SPR3}* fragment was amplified with TN110 and TN111, digested with *Sac*I and *Not*I, and cloned into pRS424-T_{CYC1} to generate pRS424-P_{SPR3}-T_{CYC1}. Third, the *GFP-SPO20$^{51–91}$-linker* fragment, coding GFP-Spo20$^{51–91}$ followed by a flexible linker, $[Ser–Ala–Gly–Gly]_4$ ([SAGG]×4), was amplified with TN27 and TN100 using pRS424-P_{TEF1}-GFP-SPO20$^{51–91}$ as a template, digested with *Not*I and *Bam*HI, and cloned into pRS424-P_{SPR3}-T_{CYC1} to generate pRS424-P_{SPR3}-GFP-SPO20$^{51–91}$-[SAGG]×4-T_{CYC1}. Finally, *GIP1-C1* to *C3* fragments were amplified with indicated primers, digested with *Bam*HI and *Xho*I, and cloned into pRS424-P_{SPR3}-GFP-SPO20$^{51–91}$-[SAGG]×4-T_{CYC1}.

To generate pRS424-P_{SPR3}-GFP-SPO20$^{51–91}$-GLC7, the *GLC7* fragment was amplified with YO255 and YO256, digested with *Bam*HI and *Pst*I, and cloned into pRS424-P_{SPR3}-GFP-SPO20$^{51–91}$-[SAGG]×4-T_{CYC1}. pRS426-GIP1-C1-mCherry was generated as follows: First, the *mCherry* fragment was cut out from pFA6a-mCherry-HIS3MX6 with *Pac*I and *Bgl*II, and the *GIP1* fragment was cut out from pRS424-GIP1-GFP with *Xho*I and *Pac*I and cloned into *Xho*I- and *Bgl*II-digested pRS424-GIP1-GFP to generate pRS424-GIP1-mCherry. Second, the *GIP1-C1-mcherry* fragment was cut out from pRS424-GIP1-mCherry with *Eco*RI and *Sac*II, and the *GIP1-C1* fragment was cut out from pRS424-GIP1-C1-GFP with *Xho*I and *Eco*RI and cloned into *Xho*I- and *Sac*II-digested pRS426.

pRS424-VPS13-GFP was generated as follows: First, the *GFP-*T_{ADH1} fragment was amplified using YSMO017 and YSMO018, with pFA6a-GFP(S65T)-kanMX6 as a template, digested with *Xho*I and *Kpn*I, and cloned into pRS424 to generate pRS424-C-GFP-T_{ADH1}. Second, the *VPS13* fragment was amplified with TN194 and TN211, digested with *Sac*I and *Xho*I, and cloned into pRS424-C-GFP-T_{ADH1}.

Sporulation

Sporulation was performed as previously described (Neiman, 1998). For sporulation on plates, cells grown on yeast extract–peptone–dextrose (YPD) or synthetic dextrose (SD) medium plates were shifted to sporulation plates (1% potassium acetate) and incubated at 30°C.

Microscopy

Differential interference contrast (DIC) images and fluorescence images were obtained with a BX71 microscope (Olympus, Tokyo,

Japan), a Quantix 1400 camera (Photometrics), and IPLab 3.7 software (Scanalytics).

Nuclear capture counting and prospore membrane perimeter measurement were performed as previously described (Okumura *et al.*, 2016). Cells expressing both Htb2-mCherry and GFP-Spo20$^{51–91}$ were sporulated for 9 h, and postmeiotic cells were identified by the pattern of Htb2-mCherry localization. The percentage of prospore membranes capturing nuclei is shown for each strain. Prospore membrane perimeters were measured by ImageJ (http://rsb.info.nih.gov/ij/).

Time-lapse imaging was performed as previously described (Ishihara *et al.*, 2009). Images were captured on a Zeiss Axiovert 100 microscope (Carl Zeiss, Oberkochen, Germany) equipped with a CoolSNAP HQ camera (Photometrics) at 2-min intervals with IPLab 3.6.5a software (Scanalytics). The temperature was held at 28°C during image collection. Three-dimensional stacks were performed with IPLab 3.6.5a.

Prediction of secondary structure, helix, and NLS

JPred4 (http://www.compbio.dundee.ac.uk/jpred4/index.html), PSIPRED (http://bioinf.cs.ucl.ac.uk/psipred/), and XtalPred (http://ffas.burnham.org/XtalPred-cgi/xtal.pl) were used to predict the secondary structure of Gip1. HeliQuest (http://heliquest.ipmc.cnrs.fr/) was used to predict the structure of the helix. cNLS mapper (http://nls-mapper.iab.keio.ac.jp/cgi-bin/NLS_Mapper_form.cgi) was used to predict the NLS of Gip1.

Dityrosine fluorescence assay

The dityrosine fluorescence assay was performed as previously described (Suda *et al.*, 2009). Briefly, cells were sporulated on filter paper for 2 d. This filter paper was treated with 10% ammonia solution and exposed to ultraviolet light to detect dityrosine fluorescence.

Ethanol-resistance assay

The ethanol-resistance assay was performed as previously described (Ishihara *et al.*, 2009). Cells were sporulated for 2 d, and 1×10^6 cells of each transformants were incubated in 400 µl sterile water (control) or 540 µl 26% ethanol for 40 min and inoculated onto YPD plates. These plates were incubated for 2 d.

Western blot analysis

The sporulating cultures were treated with trichloroacetic acid (TCA) (final concentration: 6%) on ice for 15 min. Samples were centrifuged at 15,000 rpm for 5 min, washed in 70% ethanol, and stored at –80°C. Samples were resuspended into urea buffer (6 M urea, 50 mM Tris-HCl [pH 7.5], 5 mM EDTA, 1% SDS, 1 mM phenylmethylsulfonyl fluoride) and vortexed with a multibead shocker eight times for 30 s to crash cells.

Samples were incubated at 65°C for 10 min and centrifuged at 15,000 rpm for 5 min, and supernatant was harvested. Samples of 20 µl equivalent of OD_{600} = 0.2 culture were mixed with 10 µl 3×SDS sample buffer (150 mM Tris-HCl [pH 6.8], 6% SDS, 18% β-mercaptoethanol, 30% glycerol, 0.3 mg/ml bromophenol blue), and 18 µl of the mixture was loaded into SDS–PAGE electrophoresis.

For analysis of phosphorylation, TCA-treated samples were harvested as mentioned above, except for resuspension into EDTA-free urea buffer. The CIAP (2250A; Takara, Siga, Japan) reaction was performed in a reacting buffer (1.2 M urea, 100 mM Tris-HCl [pH 7.5], 1 mM $MgCl_2$, protease inhibitor cocktail [Roche, Basel, Switzerland]) for 1 h at 37°C.

Proteins separated on SDS–PAGE gel were transferred to a polyvinylidene difluoride membrane. Membranes were blocked in 5% skim milk in TBS/T (Tris-buffered saline, 50 mM Tris-HCl [pH 7.5], 150 mM NaCl, 0.1% Tween-20) for 1 h. Membranes were probed for 1 h with the primary antibody, a 1:100 dilution of monoclonal anti-hemagglutinin (HA) monoclonal antibody (mAb; 12CA5; Roche) or a 1:500 anti-Pgk1 mAb (459250; Thermo Scientific). After being washed three times with TBS/T for 10 min, membranes were treated with the horseradish peroxidase–conjugated secondary antibody (A9044; Sigma-Aldrich) for 1 h. After being washed three times with TBS/T for 10 min, the membrane was treated with ImmunoStar LD (296-69901; Wako, Osaka, Japan), and images were obtained with an ImageQuant LAS-4000mini (GE Healthcare, Little Chalfont, UK).

ACKNOWLEDGMENTS

We thank Kazushige Touhara for helpful discussions. We also thank Takahiro Ohira for technical assistance. This work was supported by Japan Society for the Promotion of Science KAKENHI Grants JP25450094 and JP17K07712 to H.T. and National Institutes of Health Grant R01 GM-072540 to A.M.N.

REFERENCES

Adams A, Gottschling DE, Kaiser CA, Stearns T (1997). Methods in Yeast Genetics, New York: Cold Spring Harbor Laboratory Press.

Akiyoshi B, Nelson CR, Ranish JA, Biggins S (2009). Quantitative proteomic analysis of purified yeast kinetochores identifies a PP1 regulatory subunit. Genes Dev 23, 2887–2899.

Bajgier BK, Malzone M, Nickas M, Neiman AM (2001). *SPO21* is required for meiosis-specific modification of the spindle pole body in yeast. Mol Biol Cell 12, 1611–1621.

Bertin A, McMurray MA, Grob P, Park S-S, Garcia G, Patanwala I, Ng H-L, Alber T, Thorner J, Nogales E (2008). *Saccharomyces cerevisiae* septins: supramolecular organization of heterooligomers and the mechanism of filament assembly. Proc Natl Acad Sci USA 105, 8274–8279.

Bertin A, McMurray MA, Pierson J, Thai L, McDonald KL, Zehr EA, Garcia G, Peters P, Thorner J, Nogales E (2012). Three-dimensional ultrastructure of the septin filament network in *Saccharomyces cerevisiae*. Mol Biol Cell 23, 423–432.

Bollen M, Peti W, Ragusa MJ, Beullens M (2010). The extended PP1 toolkit: designed to create specificity. Trends Biochem Sci 35, 450–458.

Bridges AA, Zhang H, Mehta SB, Occhipinti P, Tani T, Gladfelter AS (2014). Septin assemblies form by diffusion-driven annealing on membranes. Proc Natl Acad Sci USA 111, 2146–2151.

Briza P, Breitenbach M, Ellinger A, Segall J (1990). Isolation of two developmentally regulated genes involved in spore wall maturation in *Saccharomyces cerevisiae*. Genes Dev 4, 1775–1789.

Bryant NJ, James DE (2003). The Sec1p/Munc18 (SM) protein, Vps45p, cycles on and off membranes during vesicle transport. J Cell Biol 161, 691–696.

Cannon JF (2010). Function of protein phosphatase-1, Glc7, in *Saccharomyces cerevisiae*. Adv Appl Microbiol 73, 27–59.

Chi RJ, Torres OT, Segarra VA, Lansley T, Chang JS, Newpher TM, Lemmon SK (2012). Role of Scd5, a protein phosphatase-1 targeting protein, in phosphoregulation of Sla1 during endocytosis. J Cell Sci 125, 4728–4739.

Christianson TW, Sikorski RS, Dante M, Shero JH, Hieter P (1992). Multifunctional yeast high-copy-number shuttle vectors. Gene 110, 119–122.

De Virgilio C, DeMarini DJ, Pringle JR (1996). *SPR28*, a sixth member of the septin gene family in *Saccharomyces cerevisiae* that is expressed specifically in sporulating cells. Microbiology 142, 2897–2905.

Diamond AE, Park J-S, Inoue I, Tachikawa H, Neiman AM (2009). The anaphase promoting complex targeting subunit Ama1 links meiotic exit to cytokinesis during sporulation in *Saccharomyces cerevisiae*. Mol Biol Cell 20, 134–145.

Engel ER, Dietrich FS, Fisk DG, Binkley G, Balakrishnan R, Costanzo C, Dwight SS, Hitz BC, Karra K, Nash RS, *et al.* (2014). The reference genome sequence of *Saccharomyces cerevisiae*: then and now. G3 (Bethesda) 4, 389–398.

Fares H, Goetsch L, Pringle JR (1996). Identification of a developmentally regulated septin and involvement of the septins in spore formation in *Saccharomyces cerevisiae*. J Cell Biol 132, 399–411.
Finnigan GC, Booth EA, Duvalyan A, Liao EN, Thorner J (2015). The carboxy-terminal tails of septins Cdc11 and Shs1 recruit myosin-II binding factor Bni5 to the bud neck in *Saccharomyces cerevisiae*. Genetics 200, 843–862.
Finnigan GC, Sterling SM, Duvalyan A, Liao EN, Sargsyan A, Garcia G, Nogales E, Thorner J (2016). Coordinate action of distinct sequence elements localizes checkpoint kinase Hsl1 to the septin collar at the bud neck in *Saccharomyces cerevisiae*. Mol Biol Cell 27, 2213–2233.
Gao J, Takeuchi H, Zhang Z, Fukuda M, Hirata M (2012). Phospholipase C-related but catalytically inactive protein (PRIP) modulates synaptosomal-associated protein 25 (SNAP-25) phosphorylation and exocytosis. J Biol Chem 287, 10565–10578.
Garcia G, Finnigan GC, Heasley LR, Sterling SM, Aggarwal A, Pearson CG, Nogales E, McMurray MA, Thorner J (2016). Assembly, molecular organization, and membrane-binding properties of development-specific septins. J Cell Biol 212, 515–529.
Gardiner FC, Costa R, Ayscough KR (2007). Nucleocytoplasmic trafficking is required for functioning of the adaptor protein Sla1p in endocytosis. Traffic 8, 347–358.
Heasley LR, McMurray MA (2016). Roles of septins in prospore membrane morphogenesis and spore wall assembly in *Saccharomyces cerevisiae*. Mol Biol Cell 27, 442–450.
Ishihara M, Suda Y, Inoue I, Tanaka T, Takahashi T, Gao XD, Fukui Y, Ihara S, Neiman AM, Tachikawa H (2009). Protein phosphatase type 1-interacting protein Ysw1 is involved in proper septin organization and prospore membrane formation during sporulation. Eukaryot Cell 8, 1027–1037.
Knop M, Strasser K (2000). Role of the spindle pole body of yeast in mediating assembly of the prospore membrane during meiosis. EMBO J 19, 3657–3667.
Kozubowski L, Panek H, Rosenthal A, Bloecher A, DeMarini DJ, Tatchell K (2003). A Bni4–Glc7 phosphatase complex that recruits chitin synthase to the site of bud emergence. Mol Biol Cell 14, 26–39.
Kupiec M, Byers B, Esposito RE, Mitchell AP (1997). Meiosis and sporulation in *Saccharomyces cerevisiae*. In: The Molecular and Cellular Biology of the Yeast *Saccharomyces*, ed. J.R Pringle, J.R Broach, and E. Jones, Cold Spring Harbor, NY: Cold Spring Harbor Laboratory Press, 889–1036.
Lam C, Santore E, Lavoie E, Needleman L, Fiacco N, Kim C, Neiman AM (2014). A visual screen of protein localization during sporulation identifies new components of prospore membrane-associated complexes in budding yeast. Eukaryot Cell 13, 383–391.
Longtine MS, McKenzie A, Demarini DJ, Shah NG, Wach A, Brachat A, Philippsen P, Pringle JR (1998). Additional modules for versatile and economical PCR-based gene deletion and modification in *Saccharomyces cerevisiae*. Yeast 14, 953–961.
Mathieson EM, Suda Y, Nickas M, Snydsman B, Davis TN, Muller EGD, Neiman AM (2010). Vesicle docking to the spindle pole body is necessary to recruit the exocyst during membrane formation in *Saccharomyces cerevisiae*. Mol Biol Cell 21, 3693–3707.
Meitinger F, Palani S, Hub B, Pereira G (2013). Dual function of the NDR-kinase Dbf2 in the regulation of the F-BAR protein Hof1 during cytokinesis. Mol Biol Cell 24, 1290–1304.
Moens PB (1971). Fine structure of ascospore development in the yeast *Saccharomyces cerevisiae*. Can J Microbiol 17, 507–510.
Moreno-Borchart AC, Strasser K, Finkbeiner MG, Shevchenko A, Shevchenko A, Knop M (2002). Prospore membrane formation linked to the leading edge protein (LEP) coat assembly. EMBO J 20, 6946–6957.
Nakanishi H, de los Santos P, Neiman AM (2004). Positive and negative regulation of a SNARE protein by control of intracellular localization. Mol Biol Cell 15, 1802–1815.
Nakanishi H, Morishita M, Schwartz CL, Coluccio A, Engebrecht J, Neiman AM (2006). Phospholipase D and the SNARE Sso1p are necessary for vesicle fusion during sporulation in yeast. J Cell Sci 119, 1406–1415.
Neiman AM (1998). Prospore membrane formation defines a developmentally regulated branch of the secretory pathway in yeast. J Cell Biol 140, 29–37.
Neiman AM (2005). Ascospore formation in the yeast *Saccharomyces cerevisiae*. Microbiol Mol Biol Rev 69, 565–584.
Neiman AM (2011). Sporulation in the budding yeast *Saccharomyces cerevisiae*. Genetics 189, 737–765.
Neiman AM, Katz L, Brennwald PJ (2000). Identification of domains required for developmentally regulated SNARE function in *Saccharomyces cerevisiae*. Genetics 155, 1643–1655.
Nickas ME, Neiman AM (2002). Ady3p links spindle pole body function to spore wall synthesis in *Saccharomyces cerevisiae*. Genetics 160, 1439–1450.
Nickas ME, Schwartz C, Neiman AM (2003). Ady4p and Spo74p are components of the meiotic spindle pole body that promote growth of the prospore membrane in *Saccharomyces cerevisiae*. Eukaryot Cell 2, 431–445.
Okumura Y, Nakamura TS, Tanaka T, Inoue I, Suda Y, Takahashi T, Nakanishi H, Nakamura S, Gao X, Tachikawa H (2016). The dysferlin domain-only protein, Spo73, is required for prospore membrane extension in *Saccharomyces cerevisiae*. mSphere 1, e00038–15.
Park J-S, Neiman AM (2012). *VPS13* regulates membrane morphogenesis during sporulation in *Saccharomyces cerevisiae*. J Cell Sci 125, 3004–3011.
Park J-S, Okumura Y, Tachikawa H, Neiman AM (2013). *SPO71* encodes a developmental stage-specific partner for Vps13 in *Saccharomyces cerevisiae*. Eukaryot Cell 12, 1530–1537.
Park J-S, Thorsness MK, Policastro R, McGoldrick LL, Hollingsworth NM, Thorsness PE, Neiman AM (2016). Yeast Vps13 promotes mitochondrial function and is localized at membrane contact sites. Mol Biol Cell 27, 2435–2449.
Parodi EM, Baker CS, Tetzlaff C, Villahermosa S, Huang LS (2012). *SPO71* mediates prospore membrane size and maturation in *Saccharomyces cerevisiae*. Eukaryot Cell 11, 1191–1200.
Parodi EM, Roesner JM, Huang LS (2015). *SPO73* and *SPO71* function cooperatively in prospore membrane elongation during sporulation in *Saccharomyces cerevisiae*. PLoS One 10, e0143571.
Peters C, Andrews PD, Stark MJ, Cesaro-Tadic S, Glatz A, Podtelejnikov A, Mann M, Mayer A (1999). Control of the terminal step of intracellular membrane fusion by protein phosphatase 1. Science 285, 1084–1087.
Sanz P, Alms GR, Haystead TA, Carlson M (2000). Regulatory interactions between the Reg1–Glc7 protein phosphatase and the Snf1 protein kinase. Mol Cell Biol 20, 1321–1328.
Schimmang T, Tollervey D, Kern H, Frank R, Hurt EC (1989). A yeast nucleolar protein related to mammalian fibrillarin is associated with small nucleolar RNA and is essential for viability. EMBO J 8, 4015–4024.
Segrest JP, De Loof H, Dohlman JG, Brouillette CG, Anantharamaiah GM (1990). Amphipathic helix motif: classes and properties. Proteins Struct Funct Genet 8, 103–117.
Sikorski RS, Hieter P (1989). A system of shuttle vectors and yeast host strains designed for efficient manipulation of DNA in *Saccharomyces cerevisiae*. Genetics 122, 19–27.
Stuart JS, Frederick DL, Varner CM, Tatchell K (1994). The mutant type 1 protein phosphatase encoded by *glc7-1* from *Saccharomyces cerevisiae* fails to interact productively with the *GAC1*-encoded regulatory subunit. Mol Cell Biol 14, 896–905.
Suda Y, Rodriguez RK, Coluccio AE, Neiman AM (2009). A screen for spore wall permeability mutants identifies a secreted protease required for proper spore wall assembly. PLoS One 4, e7184.
Tachikawa H, Bloecher A, Tatchell K, Neiman AM (2001). A Gip1p-Glc7p phosphatase complex regulates septin organization and spore wall formation. J Cell Biol 155, 797–808.
Tu J, Carlson M (1995). REG1 binds to protein phosphatase type 1 and regulates glucose repression in *Saccharomyces cerevisiae*. EMBO J 14, 5939–5946.
Tu JL, Song WJ, Carlson M (1996). Protein phosphatase type-1 interacts with proteins required for meiosis and other cellular processes in *Saccharomyces cerevisiae*. Mol Cell Biol 16, 4199–4206.
Wu H, Guo J, Zhou Y-T, Gao X-D (2015). The anillin-related region of Bud4 is the major functional determinant for Bud4's function in septin organization during bud growth and axial bud site selection in budding yeast. Eukaryot Cell 14, 241–251.